

**Low-frequency internal oceanic  
variability under seasonal forcing**

**Paul G. Myers and Andrew J. Weaver**

**C<sup>2</sup>GCR Report No. 91-19**

**November 1991**

# Low-frequency internal oceanic variability under seasonal forcing

Paul G. Myers and Andrew J. Weaver

Department of Meteorology  
and  
Centre for Climate and Global Change Research  
McGill University  
805 Sherbrooke St. West  
Montreal, P.Q., H3A 2K6  
Canada

Submitted to:  
*Journal of Geophysical Research - Oceans*  
November, 1991

## Abstract

A series of numerical experiments are conducted using the Bryan-Cox Ocean General Circulation Model to investigate the potential existence of low-frequency variability of the thermohaline circulation under seasonal forcing. Experiments are performed with different combinations of a seasonal cycle being present or not on the restoring temperature and the surface freshwater flux fields (mixed boundary conditions).

Despite the presence of the forcing on the dominant seasonal timescale, it is found that the system may oscillate at the decadal period or longer. The decadal variability is excited by changes in the net surface density flux which are due to the advection of temperature and salinity anomalies in the model domain. The magnitude of the seasonal cycle also plays an important role in determining the timescale of variability. Violent overturning events  $O(80+ Sv)$  may occur on the century timescale under seasonal forcing. The magnitudes of the flushes are reduced compared to those found in similar experiments without the presence of a seasonal cycle.

## 1.0 Introduction

Over the last few years interest in studying the effects of variability in the climate system has grown as it has been realized that the Earth's climate has exhibited large changes in the past (Crowley, 1988) and will probably continue to change in the future. Variability exists in all five components of the climate system: the atmosphere, hydrosphere, cryosphere, lithosphere and biosphere, although on widely different timescales. These components are all coupled, with any variability in one component able to force changes, that are global in scale, in some or all of the other components.

There are two types of this variability; for example in the ocean, variations in its external forcing (such as solar heating, winds, evaporation/precipitation, etc) can cause variability. Then there is the internal variability of the oceanic system itself. The ocean plays a key role in climate due to its high heat capacity which acts as a thermal buffer, and due to its role in the transfer of heat from equatorial regions to high latitudes.

Numerous observations of low-frequency variability in the air-sea-ice climate system have been found in recent years. For example, variations on the decadal/interdecadal timescale have been observed in global surface air temperatures (Ghil & Vautard, 1991), West African rainfall and the landfall of intense hurricanes on the US coast (Gray, 1990), Arctic sea ice extent (Mysak & Manak, 1989; Mysak et al., 1990), runoff from the Eurasian land mass (Cattle, 1985; Ikeda, 1990) and global sea level pressure (Krishnamurti et al., 1986). Decadal/interdecadal variability has also been observed in the properties of the North Atlantic Deep Water (NADW) formation (Schlosser et al., 1991; Lazier, 1980; Dickson et al., 1988) which have important implications for the thermohaline

circulation (THC) and hence oceanic poleward heat transport.

Recently, Ocean General Circulation Models (OGCMs) have been used to examine the stability and variability properties of the thermohaline circulation. Many of these studies have evolved from the pioneering work of F. Bryan (1987) who showed how multiple equilibrium of the thermohaline circulation could exist in the Bryan-Cox OGCM under mixed boundary conditions (a restoring boundary condition on temperature and a fixed flux on salinity).

In a few of the experiments of Marotzke (1990) and in the works of Weaver and Sarachik (1991a,b) and Weaver et al. (1991a,b), spontaneous variability of the thermohaline circulation was found with a decadal timescale. This variability was shown to be characterized by the generation and advection of salinity and temperature anomalies which affected the deep water formation. More detail of the mechanism involved in the generation and advection of these anomalies is given in Weaver and Sarachik (1991b).

Marotzke (1990) observed another phenomenon in his 2-dimensional and 3-dimensional models. In the absence of wind forcing the thermohaline circulation could collapse, leading eventually to a period of intense convection during which the overturning increased to a strength of  $O(150 \text{ Sv})$ . Weaver and Sarachik (1991a), who included wind forcing, and Wright and Stocker (1991) who did not, also observed a similar phenomenon and showed that when the circulation was in a collapsed state, low latitude diffusion and the subsequent horizontal homogenization warmed the deep ocean past a certain critical point. This made the deep waters lighter than the overlying waters at high latitudes, thereby causing static instability, convection and a rapid loss of much of the heat that the basin had built-up in its collapsed state. The event was termed a flush.

In all of these studies, steady forcing was used. The radiant

energy that drives the earth's fluid envelopes comes from the sun. This energy is not constant at any given latitude, but varies on numerous timescales, with seasonal variations having important effects on the mean state of the atmosphere and ocean (Gill,1982). Changing from annual mean insolation to seasonal forcing has been demonstrated to change the mean state of a numerical model (Wetherald&Manabe,1972). So, is the presence of decadal/interdecadal variability in models that lack a seasonal cycle an artifact of the these annually-averaged boundary conditions or not? To this effect, we will in this paper go one step further and consider non-steady periodic forcing. We show that decadal variability, internal to the system, can exist even in the presence of non-steady seasonal forcing.

The outline of this paper is as follows. In section 2 we briefly describe the numerical model; in section 3 we introduce and discuss the numerical experiments that were performed, and in section 4 we examine the effect different boundary conditions have on the poleward heat transport. We summarize our results in section 5.

## 2.0 Description of the Numerical Model

We use the Cox (1984) version of the Bryan-Cox Ocean General Circulation Model to simulate a 4° latitudinal by 3.75° longitudinal horizontal resolution, 4500 m deep, flat-bottomed ocean. The domain consists of a 60° wide (southern hemisphere) basin extending from the equator to 72° S. The vertical structure consists of fifteen levels of increasing  $\Delta z$  (Table 1).

A symmetry condition is applied at the equator. No-slip and insulating conditions are used at the lateral walls. The bottom is assumed to be impermeable and insulating, while the rigid-lid approximation is used at the surface. We use a simple analytic formula for the zonal windstress which is a function of latitude only (F. Bryan, 1987).

$$(1) \tau^{\lambda}(\Phi) = 0.2 + 0.8 \sin(6\Phi) - \frac{1}{2}(1 + \tanh(10\Phi)) - \frac{1}{2}(1 + \tanh(10(\frac{\pi}{2} + \Phi))) \text{ dynes/cm}^2$$

Here  $\lambda$  is the longitude and  $\Phi$  is the latitude in radians. Despite its simplicity, this scheme captures the major features of the observed zonally averaged zonal wind stress (see Fig. 1a of Weaver and Sarachik, 1990). For simplicity there is no meridional windstress forcing. Annually averaged winds are used for reasons discussed later.

The vertical eddy diffusivity and viscosity are everywhere set to  $A_{TV} = 1.0 \text{ cm}^2/\text{s}$  and  $A_{MV} = 10.0 \text{ cm}^2/\text{s}$  whereas the horizontal eddy viscosity and diffusivity are chosen to be  $A_{MH} = 2.5 \times 10^9$  and  $A_{TH} = 2 \times 10^7 \text{ cm}^2/\text{s}$ , respectively, over the whole domain. In all experiments, the Cox (1984) implicit convection parameterization scheme is used. When the density profile is determined to be statically unstable, the vertical diffusivity  $A_{TV}$  is set to  $10^4 \text{ cm}^2/\text{s}$  for one timestep.

For all experiments the model was spun up from a resting

homogeneous ocean with uniform temperature of 5° C and salinity of 34 ppt. The surface boundary condition on temperature is a Newtonian (restoring) condition with a relaxation constant of 25 days. That is, the temperature of the first model level is relaxed to a zonally uniform reference temperature, based on the Haney (1971) formulation. We vary this reference temperature in time with a period of a year to simulate the change in temperature over the course of a year.

At the southern boundary, the reference temperature was determined by a simple analytic cosine function designed to simulate a seasonal cycle (Fig. 1a).

$$(2) \quad T_{pol} = (\cos(t*\pi/182.5+\pi)+1) * (T_{summer}/2)$$

Here  $t$  is the day of the year,  $T_{pol}$  is the temperature at the polar boundary (0°C in the winter at  $t=0$ ) and  $T_{summer}$  (6.5°C) is the maximum temperature at the polar boundary in the summer. These values were composited from the Levitus (1982) atlas of world ocean data. A 365 day year is also assumed. As the observed magnitude of the seasonal variance in temperature at the equator is small (about 1° C; Levitus, 1982), we assume a constant equatorial restoring temperature for simplicity. A cosine curve was further fitted to the equatorial and polar temperatures to obtain interpolated temperatures at intermediate latitudes. The temperatures are illustrated in Fig. 1b for spring ( $t=91$ , end of Mar.), summer ( $t=183$ , end of Jun.), fall ( $t=274$ , end of Sep.) and winter ( $t=365$ , end of Dec).

An annually averaged restoring salinity surface boundary condition was used for the spin-up. The reference salinities were obtained by compositing annually-averaged data from the Levitus (1982) atlas. No seasonal cycle was used on the restoring salinities during the spin-up so that we could focus on a minimum

number of processes. We chose to use the seasonal cycle on temperature as much more is known about the thermal seasonal cycle than the freshwater flux seasonal cycle. Furthermore, we may still obtain a seasonal cycle on freshwater flux indirectly by diagnosing this over one year at our seasonal equilibrium.

To speed up convergence of the model the acceleration techniques (asynchronous integration) of Bryan (1984) were used. The barotropic vorticity and baroclinic velocity equations were integrated with a timestep of 2 hours, while the tracer timestep was either 2.5 or 1.25 days, throughout the water column. We discuss several synchronous integration results later.

The model was integrated for 6000 surface years until a steady seasonal cycle circulation had been reached. There were no trends in the salinity, temperature or overturning streamfunction fields at the seasonal equilibrium. The model was then integrated for a further year during which the surface freshwater flux was diagnosed at each gridpoint of the basin and at each timestep for each different tracer timestep used. Slight differences existed between the freshwater fluxes diagnosed with different timesteps due to both the dependence of convection on the timestep (Weaver & Sarachik, 1991a) and to more intermediate points being used over the course of a year in the restoring temperature boundary condition under the smaller timestep. These differences do not have a significant effect on the results. So as not to have any net salt gain or loss into the basin over the course of one year, we compute this net annual salt flux and subtracted this small quantity from each gridbox at each timestep throughout the year. An instantaneously diagnosed freshwater flux is used instead of one obtained from an average over a further number of years of integration, as the differences between the two are insignificant (Weaver et. al., 1991b). The use of asynchronous integration during

the diagnosis was also shown to have no effect on the results. All experiments were integrated for a further 6000 years under mixed boundary conditions.

### 3.0 The Numerical Experiments

In this section the numerical experiments are described. A complete list of these experiments, together with their distinguishing characteristics can be found in Table 2. All experiments exhibit internal low-frequency variability of one kind or another. We shall show that this variability is a high latitude phenomenon linked inherently to the convection process. The magnitude and period of the variability depend on the nature of the surface boundary condition used and will be discussed in the following sections.

#### 3.1 Spin-up

The basin was spun-up for 6000 years until it had reached a seasonal equilibrium. The circulation is characterized by strong overturning. Although the net basin averaged surface heat flux varies greatly seasonally, there are no major seasonal variations in the overturning streamfunction between winter (Fig. 2a) and summer (Fig. 2b). The slight differences which are observed are due to the weakening of convection in the summer, leaving advection as the only process forming deep water. The process of decreased summer convection tended to reduce the zonal pressure gradients in the upper levels in summer which subsequently reduced the meridional overturning slightly. Due to the large inertia of the overturning, this seasonal convection was not able to significantly effect the mean advective deep water formation process, with net effect that the bottom water temperatures reflect mean 'spring/fall' conditions (Table 3).

The seasonal changes in the surface heat flux are directly due to the changes in the restoring temperature, causing the ocean to lose much more heat to the colder "atmosphere" in the winter ( $62.7 \text{ W/m}^2$  basin averaged at equilibrium) and to gain heat from the "atmosphere" in the summer ( $42.5 \text{ W/m}^2$  basin averaged at

equilibrium). Seasonal changes are seen in the upper levels of the zonal temperature fields, with the presence of a sharp seasonal thermocline in the summer (Fig. 2c) changing in winter, at high latitudes, to the near vertical isotherms representative of convective activity (Fig. 2d).

We calculated the net density flux into the basin for each season (Fig. 3a-d) and for the annual average case (Fig. 3e). These calculations are based on the formulae in Schmitt et al. (1989). The density flux  $F_\rho$ , is given by  $F_\rho = -\rho(\alpha F_T - \beta F_S)$  where  $\rho$  is the density, and the thermal expansion and haline contraction coefficients are defined by

$$\alpha = -\frac{1}{\rho} \frac{\partial \rho}{\partial T} \Big|_{P,S} \quad , \quad \beta = \frac{1}{\rho} \frac{\partial \rho}{\partial S} \Big|_{P,T} .$$

Here  $F_T = Q/\rho C_p$  where  $Q$  is the net heat flux into the ocean and  $C_p$  is the heat capacity of water. The flux of salt is due to the loss of fresh water from the sea surface and is given by  $F_S = S(E - P)/(1 - S)$ .  $(E - P)$  is the freshwater flux in m/s and  $S$  is the salinity given in kilograms salt per kilogram water. For these calculations the expansion coefficients, heat capacity and densities were evaluated using the surface temperature and salinity appropriate for the latitude, longitude and time of year.

Our figures fortuitously agree quite well with those of Schmitt et al. (1989) in a qualitative sense. In the annual mean, they reveal a net density loss in the subtropical gyre, with density gains at higher latitudes and along the western boundary (Fig. 3e). The density gain is greatest in the winter (Fig. 3d) due to the lower restoring temperatures. This is especially true in the high latitude regions. During the spring (Fig. 3a) and the summer (Fig. 3b) there is a net density loss over almost the entire basin. In the fall (Fig. 3c), with the onset of deep convection at high latitudes, there is a more intensified density gain there.

The individual contributions of heat and salt to the density flux are shown in Fig. 3f, as the absolute value of the thermal/haline ratio ( $|\alpha F_T/\beta F_S|$ ). This confirms that the restoring boundary condition equilibrium is thermally controlled. Again, our results agree well with those of Schmitt et al. (1991), with temperature dominating near the equator and in the high latitude regions. The lack of a region of salinity domination in the subtropics is probably due to the poor parameterization of small scale mixing processes in the model, which are believed to play a key role in the real ocean (Schmitt et al., 1991).

### 3.2 Experiment 1

This experiment is a control run where no seasonal cycle is present on either temperature or the freshwater flux. A constant temperature of 0°C is used at the polar boundary. This temperature was chosen to allow for the development of a strong overturning circulation. An annual freshwater flux is used (Fig. 4). We term this our *Perpetual Winter* experiment.

Upon switching boundary conditions from restoring to mixed, the basin immediately flushed. This followed since after the removal of the seasonal cycle on temperature that was used during the spin-up, we now forced the surface waters with the 0°C temperature. This produced an unstable situation, with cool dense water overlying the warmer and lighter deep water produced during the spin-up. This led to the basin flushing. The circulation then settled down to a seasonal equilibrium with low magnitude oscillations of less than 0.5 W/m<sup>2</sup>. Strong decadal variability is not excited due to the lack of a local maximum away from the southern boundary at high latitudes in the density flux field (not shown). Instead, the density flux field increased monotonically towards the southern boundary, with the maximum right at the southern wall.

### 3.3 Experiment 2

In this, our *Fully Seasonal* experiment, we use the freshwater flux diagnosed from the spinup every timestep, and allow it to vary over the course of the year to simulate a seasonal cycle on the freshwater flux forcing. Figs. 5(a-d) show the variations of the freshwater flux forcing field over the course of a year.

Characterizing the fields are low latitude evaporation and high latitude freshening. Intense precipitation occurs between 40°S and 70°S in winter (Fig. 5d) but is counteracted by a weakening of the precipitation during the rest of the year. In fact, an evaporative region forms in the summer (Fig. 5b). These occurrences are due to the presence of the restoring boundary condition on salinity during the spin-up. At high latitudes, the restoring salinity falls between the predicted surface salinities for the summer and the winter. At the start of the summer the surface waters are relatively fresh due to the absence of convection, with a salinity less than the restoring value. This leads to the model diagnosing the band of evaporation seen in Fig. 5b. During the winter the processes of convection and advection act to produce a pool of water with surface salinity greater than the restoring value, which leads to the model diagnosing the precipitation seen in winter (Fig. 5d). Fortunately, our diagnosed freshwater fluxes agree quite well qualitatively with the observations of Schmitt et al. (1989).

The seasonal steady state obtained under restoring boundary conditions remained relatively stable upon the switch to mixed boundary conditions. To investigate the effects of the asynchronous integration techniques of Bryan (1984), a further integration was conducted synchronously from the end of the mixed boundary condition experiment, with a timestep of 6 hours on all equations for 1000 years. A new P-E field was diagnosed for this run. The

circulation remained stable upon the switch in timestep.

Further investigation revealed, however, that the system was not completely stable under mixed boundary conditions, for weak oscillations were superimposed on the seasonal equilibrium basic state. Changes in the overturning streamfunction were small ( $<0.1$  Sv) but the net basin averaged surface heat flux oscillated by  $\pm 2$   $\text{W/m}^2$  over a 20.83 year period (Fig. 6a). The synchronous integration confirmed this timescale but revealed a much smaller magnitude of variability, about  $0.25$   $\text{W/m}^2$  (Fig. 6b).

Furthermore, it is not clear whether the very small differences between the synchronous and asynchronous integrations are due to the change in integration procedure or are simply due to the timestep dependence on convection (Weaver & Sarachik, 1991a). Also, we use a finer interpolation on both the seasonal restoring temperature and the seasonal freshwater flux in the synchronous integration experiment, perhaps yielding the small changes in the oceanic response. Nevertheless, since these fluctuations are so small, we conclude that the restoring boundary condition seasonal equilibrium is stable upon the switch to seasonally varying mixed boundary conditions.

### 3.4 Experiment 3

In the next series of experiments, a seasonal cycle is placed on one, but not both of the surface boundary conditions. To obtain a constant annual mean, we average the seasonal freshwater fluxes over the course of the year (Fig. 4). In Exp. 3, our *Seasonal Temperature* experiment, the basin was integrated with a seasonal cycle on temperature only, with a tracer timestep of 1.25 days.

Upon the change from restoring to mixed boundary conditions, the circulation collapsed. Following this, the circulation increased in strength and began to oscillate irregularly. After several thousand years, the circulation steadied, entering a long

period of fairly regular oscillations. The net basin averaged surface heat flux taken every year at the height of the respective seasons revealed magnitudes of  $2 \text{ W/m}^2$  in the summer (Fig. 7a) and  $20 \text{ W/m}^2$  in the winter (Fig. 7b).

The corresponding power spectral densities of these time series are given in Figs. 7(c-d). They show very strong decadal peaks at around 11 years, especially in the winter, plus weaker inter-annual peaks. The series of peaks at higher frequencies in the summer plot (Fig. 7c) indicate the non-linear transfer of energy from high-frequency variability to low-frequency motion. Although it is not strictly correct to discuss timescales when using asynchronous integration, the results from the synchronous integration conducted in Exp. 4 will show that these timescales are valid.

The oscillations are characterized by changes in the meridional overturning streamfunction. Over a single cycle, deep water formation occurs and then suddenly shuts off, followed by the development of a reverse cell that increases with time (as in Weaver & Sarachik, 1991b). The whole process then repeats itself. The time needed for the full cycle is about 11 years. Figure 8 shows the development of the overturning streamfunction over an oscillation. Over the course of an oscillation the THC slowly decreases in strength by a factor of two. Although weakened, the THC never actually collapses during the oscillation. As the THC weakens, a reverse cell begins to form at the polar boundary, rapidly growing in strength until it is nearly equal in magnitude to the main cell (Fig. 8b). The reverse cell quickly fades away (Fig. 8c), leaving a strengthening main cell which continues to grow until the oscillation begins anew.

This variability is linked to the existence of a local minimum in the P-E forcing field (Fig. 4) and to cooling between  $60^\circ$  and

70° N. As the waters travel poleward, they pass through this local minimum, where they are only freshened slightly. At the same time, the waters are being cooled, which acts to oppose the freshening by increasing the density. The low restoring temperatures are cool enough to overcome the decreased freshening in the region, allowing thermal effects to dominate over the haline effects (Fig. 9a). This means we have a positive maximum of the density flux into the ocean here (Fig. 9b), which causes overturning and deep sinking here. This increases the strength of the THC, causing its waters to pass rapidly through this region, into higher latitudes where the freshening is more important. In turn, this weakens deep convection, breaking down zonal pressure gradients and hence slowing the circulation and allowing water particles to spend more time in the zone of P-E minimum. This causes the process to begin anew. A more complete description of the oscillation can be found in Weaver and Sarachik (1991b) and Myers (1991).

### 3.5 Experiment 4

In Exp. 4, our *Synchronous Seasonal Temperature* experiment, we repeated Exp. 3 but all equations were now integrated synchronously with a timestep of 6 hours. This experiment reveals that the results from the asynchronous runs are robust. Only slight differences exist between the two runs, none of which have any significant effect on the overturning streamfunction. The surface heat flux (Fig. 10a) agrees very well with that from the previous run (Fig 7b). The power spectral density of this series (not shown) revealed that the same periods of oscillation were dominant. As well, plots of the differences in zonal temperature between Exp. 3 and Exp. 4 for the summer (Fig. 10b) and winter (Fig. 10c) of a 1-year additional integration show almost no difference. The slight difference near 62°S is in the region of most marked variability during an oscillation. Due to the chaotic nature of the

oscillation, it is not surprising that we see small differences there.

The successful application of a seasonal cycle with asynchronous integration is due to our use of constant annual winds. Communication with Keith Dixon at GFDL reveals that timestep splitting works best when the winds change slowly or not at all. This is because winds, and especially variations in them, cause deviations from the basic asynchronous assumption that the velocity field is largely determined from the density field. This is especially true in coupled atmosphere-ocean models (Bryan et. al., 1975; Washington & Meehl, 1989), which are much more sensitive to the timestep splitting due to the coupling between the two components of the model. Atmospheric disturbances can cause the surface windstress boundary condition for the OGCM to change rapidly. By keeping the winds constant, we reduce the variations in the surface momentum fluxes that the surface waters are forced to respond to (K. Dixon, 1991, personal communication).

### 3.6 Experiment 5

In Exp. 3, we tested the effect of having a seasonal cycle on temperature. Now, we look at the effect of having a seasonal cycle only on the freshwater flux. This is done by keeping the polar boundary restoring temperature constant at 0°C over the entire year. A 1.25 day tracer timestep was used. We term this our *Seasonal Freshwater Flux* experiment.

The resulting behaviour of the model was quite different from that seen in the previous experiments. The circulation collapsed upon switching from restoring to mixed boundary conditions and entered a sequence of flushes and collapses, with fairly regular period. The net basin averaged surface heat flux for this run can be seen in Fig. 11a. Superimposed on this flush/collapse pattern are irregular oscillations of a fairly large magnitude. The power

spectral density of this series (Fig. 11b) reveals that the system is characterized by low-frequency oscillations on the century timescale and longer, while the smaller oscillations fall in the decadal/inter-decadal range.

At first, this result seems contradictory to Exp. 2 (*Fully Seasonal*), with its steady circulation. Both experiments have essentially the same cycle on the salinity flux. In Exp. 5 the polar boundary is kept at 0°C year round, which would seem to provide better conditions for convection and hence for a more vigorous circulation. However, near the freezing point, the density of surface water depends less upon temperature than salinity, so with the seasonal cycle on freshwater flux, convection occurs preferentially in the season when the surface freshening is the least, i.e., in the summer (Fig. 5b). With only weak convection in the winter, when freshening is strongest (Fig. 5d), a large pool of fresh water is allowed to form. Since the seasonal timescale lies between the characteristic timescales for the adjustment of the baroclinic velocity field and for density changes due to advection (Hasselmann, 1982), the density anomaly produced by the freshening will not have been advected away by the next summer, leaving a fresh water cap which will curtail convection. This process continues as a positive feedback until the circulation collapses.

In Exp. 2 where there was a seasonal cycle on temperature as well, deep convection tended to occur at the coldest period of the seasonal cycle, i.e., during the winter. Hence, the fresh water produced in that season was convected away, preventing the formation of a fresh water cap, and the excitation of the positive feedback loop. This convection was aided by the high salinity pool that was produced in the summer and not completely advected away by the winter. These mechanisms allow the maintenance of the strong, vigorous circulation that we observed in Exp. 2.

To support these ideas an analysis of convection statistics was carried out. This was accomplished by determining the grid cells, in both experiments, during both the summer and winter, in which convection occurred. In Exp. 2 (*Fully Seasonal*) we found that convection occurred exclusively in winter. Convection was found to occur in both the winter as well as the summer in Exp. 5 but was very weak and sporadic and so unable to prevent the formation of the freshwater cap that we had hypothesized.

### 3.7 Experiment 6

This experiment is similar to the *Perpetual Winter* experiment (Exp. 1) except that a different polar boundary restoring temperature is used. Here, instead of the winter temperature, we use the average temperature over the seasonal cycle used in the other experiments, i.e., 3.25°C, with the freshwater flux field from Exp. 3 (Fig. 4). We term this our *Perpetual Spring* experiment. As compared to Exp. 1, we have a weaker meridional thermal gradient, so we would expect high latitude freshening to dominate here, which is the case.

The circulation collapsed almost immediately. The basin remained in the collapsed state for a long time before a flush occurred. The system then returned to the collapsed state, slowly building up to another flush (Fig. 12a). The magnitude of the flushes were larger than those of Exp. 5 (Fig. 12b), and in fact were the largest of all experiments by almost a factor of two. Weak, irregular oscillations were superimposed on the basic structure.

The frequency of the flushes is based on a diffusive timescale, with the ocean continually gaining heat in its collapsed state. This leads to a warm salty deep ocean, which eventually becomes statically unstable, leading to ever growing convective activity at high latitudes. The excess heat gained by the basin in

the collapsed state is rapidly given off to the atmosphere.

Of interest to note is that the flushes that occurred in Exp. 5 (*Seasonal Freshwater Flux*), besides being significantly weaker, occurred at a much higher frequency than those in this experiment. Since diffusion appears to be the dominant timescale, why should the flushes occur at such different frequencies? An examination of the deep water temperatures reveals that the flushes in Exp. 6 occur when the bottom waters reached 9°C, but at only 6°C in Exp. 5. The reason is due to the presence of the seasonal cycle on the freshwater flux that exists in Exp. 5. In the constant flux case, there is high latitude freshening year round, which with the high polar restoring temperatures leads to a very stable situation. In the seasonally varying case, high latitude evaporation occurs in the late summer. This can be sufficient to cause static instability, convection and a subsequent flush. The magnitude of the flush is weaker as the deep ocean temperature is cooler, so the ocean loses less heat in the weaker flushing event. This process is similar to the strong stochastic forcing case of Weaver et al. (1991b).

### 3.8 Experiment 7

The purpose of this experiment and the following one are to investigate the effect of the magnitude of the seasonal cycle has on the results. In this, our *Amplified Seasonal Temperature* experiment, the amplitude of the cycle on temperature is increased by raising the summer temperature at the polar boundary, as is suggested, for example, to occur in the proposed greenhouse scenarios, to 9.0°C. In all other aspects, this experiment is the same as Exp. 3 (*Fully Seasonal*).

The results are however, quite different from those of Exp. 3 and in fact resemble those of Exp. 5 (*Seasonal Freshwater Flux*) most closely. With the switch in boundary conditions from restoring to

mixed, the circulation collapsed and remained quiescent for a period of time. The magnitude of the streamfunction then began to oscillate, with periods of both regularity and irregularity. After about 2000 years, the circulation went through a series of collapses and flushes, with the flushes about 350 years apart (Fig. 13a). Smaller scale oscillations in the decadal range (Fig. 13b) are superimposed on the flushes and collapses.

At low temperatures salinity dominates in the non-linear equation of state which we use (Bryan & Cox, 1972), but at higher temperatures small changes in temperature cause large changes in density. In both Exps. 3 and 7 we are always freshening at high latitudes, but in Exp. 7 it is also warmer at these high latitudes. This produces a very stable density profile at high latitudes, that cannot be compensated for by cooling in winter. This prevents strong overturning and causes the development of a polar halocline catastrophe, similar to that of F. Bryan (1987). However, over the long term, this situation is not stable with the diffusion of heat into the deep ocean, leading eventually to a flush, and the cycle then repeating itself. In Exp. 3, the lower summer temperatures do not decrease the density enough to prevent winter cooling and wind-driven salt transport from producing convection. The circulation is then allowed to re-establish itself before a flush occurs.

### 3.9 Experiment 8

In this, our *Reduced Seasonal Temperature* experiment, we lower the summer temperature at the polar boundary to 4.0°C. Otherwise, this experiment is the same as Exp. 3 (*Seasonal Temperature*). The results resembled those of Exp. 7 (*Amplified Seasonal Temperature*), with a collapse, a period of irregular oscillations, followed by a series of flushes and collapses (Fig. 14a). Small scale oscillations are also present, although at a higher frequency than those found in the previous experiment (Fig. 14b). The magnitude of the flushes

were the smallest of any experiment (Fig. 14c).

### 3.10 Summary of Experiments

In this section we showed that decadal/interdecadal variability of the THC may exist internally even in the presence of seasonal forcing. These timescales of variability are summarized in Table 3. The use of the acceleration techniques of Bryan (1984) was shown to have no important effect on the results. We were able to produce different regimes of the THC by varying the maximum temperature of the seasonal cycle. These regimes being a sequence of collapses and flushes, and a circulation showing pronounced decadal variability. Flushes were found to be weaker and more frequent than those found in experiments without a seasonal cycle.

Another effect of the inclusion of the seasonal cycle was the effect it had on bottom water temperatures (Table 3). Since most deep water is formed at the surface in high latitudes, the deep ocean is very sensitive to polar amplification of temperature (Manabe & Bryan, 1985). As one can see from the table, the bottom water temperatures increased quite markedly from Exp. 1, which was without a seasonal cycle, to those that had a seasonal cycle present, Exps. 2-4. The lower bottom temperatures in Exp. 2 (*Fully Seasonal*) are related to the lack of pronounced decadal variability in those experiments, when compared to Exps. 3 (*Seasonal Temperature*) and 4 (*Synchronous Seasonal Temperature*). In the latter two experiments, the strong oscillations in the streamfunction cause the site of deep water formation to be moved equatorward during part of the oscillation. As the surface waters are warmer at these lower latitudes where convection is now occurring, warmer water will be convected down to the deep ocean, producing warmer bottom water temperatures in Exps. 3 and 4. Since the rest of our experiments never reached a seasonal equilibrium, we do not discuss their bottom water temperatures.

#### 4.0 Poleward Heat Transport

It has been noted that a very large fraction of the oceanic heat transport can be accounted for by the thermohaline circulation (THC) (Bryan, 1962), although this does not take into consideration an important contribution from the wind (Bryan et. al., 1975). Variations in the THC can therefore have substantial effect on the poleward heat transport. In this section we will show that these oscillations in the poleward heat transport exist in our seasonal model.

Our basic poleward heat transport profile, which is for Exp. 2 (*Fully Seasonal*) is shown in Fig. 15a. It reveals slight seasonal variations in the poleward heat transport, but no interannual variations with the transport curves for each year falling directly overtop the preceding one. The lack of interannual changes are due to the fact that the THC is seasonally steady in this experiment. The same transport is shown for Exp. 1 (*Perpetual Winter*) in Fig. 15b. Again a steady THC means no interannual variations in the heat transport, while the lack of seasonal variations in the restoring temperature removes the intra-annual variations. The magnitude of the transport is stronger in the *Perpetual Winter* experiment as there is a stronger meridional temperature gradient in that experiment than in the *Fully Seasonal* experiment.

In the experiments where significant oscillations in the THC occur (Exps. 3&5), these oscillations showed up in the poleward heat transport. Figures 15(c-d) show the transport in both the summer and winter over a complete oscillation for Exp. 3 (*Seasonal Temperature*). Large variations occur over the period of the oscillation, with the maximum transport corresponding to the time when deep water is being formed at the polar boundaries and the circulation is the most vigorous. The absolute magnitude of the transport is weaker in the *Seasonal Temperature* experiment than in the

previous two because the overall circulation is weaker, and therefore less heat is be transported poleward. Similar variations were observed in Exp. 5 (*Seasonal Freshwater Flux*) (Fig. 15e), except that the variability in the transport is larger by a factor of at least two. This can be attributed to the sensitivity of convection, and therefore THC to even minor changes in the freshwater flux and the freshwater flux varies greatly over the course of this experiment.

## 5.0 Discussion and Summary

In this paper we have found that decadal variability exists under seasonal forcing. That is, despite forcing the system with a strong sub-annual signal, the system may respond with energy at the decadal or longer timescale. This result is significant as it shows that decadal variability is robust under time dependent forcing and is not an artifact of the steady surface boundary conditions used in previous models (Weaver&Sarachik, 1991a,b).

The existence of decadal/interdecadal variability in our simulation is linked to the existence of a local maxima in the net density flux forcing field. As waters pass through this region, their density is increased, causing them to sink. This sinking intensifies the overturning causing these waters to spent less time in this zone of maximum density gain. Therefore, the decrease is less, sinking is to shallower depths and the overturning is weakened. This, in turn, causes the waters to spent more time in the region of strong density gain, causing the oscillation to begin anew. The strength of the thermohaline circulation is essentially controlled by the duration of the exposure of surface waters to the region of maximum density gain.

The variability exists in our *Seasonal Temperature* experiment (Exp. 3) despite having high latitude freshening year round (Fig. 4). This implies that the oscillation is a combined temperature and salinity effect, which agrees with the results of Schmitt et al. (1989) who showed that although salt may dominate the density field at the ice/water interface, freshwater does not dominate the density fluxes in the high latitude open-ocean.

Decadal/interdecadal variability exists under both annual mean and seasonal P-E forcing. Since the P-E forcing field has large seasonal variance (Schmitt et al.,1989), this robustness is a

welcome result. Combined with the robustness found under stochastic forcing shown by Weaver et al. (1991b), this seems to show that the decadal timescale is a natural timescale of the present system.

The presence of the seasonal cycle on the freshwater flux constrains the time of year when deep convection can occur. By increasing the magnitude of the freshening that occurs in winter, the seasonally varying freshwater flux field is able to curtail convection, and cause the circulation to collapse. Although our maximum freshening is large in winter (6.7 m/year averaged zonally at high latitudes), the implications on the salinity dominated buoyancy field at these latitudes still hold.

Flushes were shown to exist under seasonal forcing. The inclusion of seasonal forcing increase the frequency of the flushes by reducing the critical temperature at which static instability occurs. As well, the flushes under seasonal forcing are weaker, producing variability in the basin averaged net surface heat flux on the order of 20-50 W/m<sup>2</sup> on the century timescale.

Our experiments with a seasonal cycle on temperature show the sensitivity of the THC to the magnitude of the summer warming. Depending on whether the summer amplitude fell within a given range or not, we were able to produce different regimes of the THC. If the summer polar restoring temperature is within this range, a steady circulation with decadal variability developed. Otherwise, it collapsed, leading to a sequence of flushes and collapses, with some decadal variability superimposed.

Another important point to mention is that even though when a seasonal cycle is present under restoring boundary conditions, the meridional overturning does not change much over the course of the year. Although convection is suppressed in the summer, thereby reducing zonal pressure gradients in the upper levels at high latitudes, the inertia of the THC is such that it remains largely

unaffected by the relatively high frequency seasonal surface forcing.

In summary, the most important conclusion of this paper is that internal variability of the THC, on decadal and longer timescales, exists even under strong seasonal forcing. Accuracy in determining the magnitudes of the seasonal cycle on temperature and freshwater flux is important as the circulation is sensitive to changes in both. The seasonal cycle also acts to curb the magnitudes of flushes and produces frequencies that may have relevance in the interpretation of long term climate records.

### Acknowledgements

This study forms the basis of PM's M.Sc. thesis, completed in the Department of Meteorology, McGill University, and was supported through NSERC, AES and FCAR operating grants awarded to AJW. We would like to thank Tertia Hughes for carefully reading an earlier version of this manuscript and providing detailed comments. PM would also like to thank Dr. William Gough for his helpful discussions and comments.

## References

- Bryan, F., 1987: Parameter sensitivity of primitive equation ocean general circulation models, *Journal of Physical Oceanography*, **17**, 970-985
- Bryan, K., 1962: Measurements of meridional heat transport by ocean currents, *Journal of Geophysical Research*, **67**, 3403-3414
- Bryan, K., 1984: Accelerating the convergence to equilibrium of ocean-climate models, *Journal of Physical Oceanography*, **14**, 666-673
- Bryan, K. and M.D. Cox, 1972: An approximate equation of state for numerical models of ocean circulation, *Journal of Physical Oceanography*, **2**, 510-514
- Bryan, K., S. Manabe and R.C. Pacanowski, 1975: A global ocean-atmosphere climate model. Part II. The oceanic circulation, *Journal of Physical Oceanography*, **5**, 30-46
- Cattle, H., 1985: Diverting Soviet rivers: Some possible repercussions for the Arctic ocean, *Polar Record*, **22**, 485-498
- Cox, M.D., 1984: A primitive equation, three-dimensional model of the ocean, GFDL Ocean Group Tech. Rep. No. 1, GFDL/NOAA, Princeton University
- Crowley, T.J., 1988: Paleoclimate Modelling, in "Physically-Based Modelling of Climate and Climate Change - Part II", ed. M.E. Schlesinger, Kluwer Academic Publishers, 883-949
- Dickson, R.R., J. Meincke, S-A Malmberg and A.J. Lee, 1988: The "Great Salinity Anomaly" in the northern North Atlantic 1968-1982, *Progress in Oceanography*, **20**, 103-151
- Ghil, M. and R. Vautard, 1991: Interdecadal oscillations and the warming trend in global temperature time series, *Nature*, **350**, 324-327
- Gill, A.E., 1982: "Atmosphere-Ocean Dynamics", Academic Press, London
- Gray, W. M., 1990: Strong association between West African rainfall and U.S. landfall of intense hurricanes, *Science*, **249**, 1251-1256
- Haney, R.L., 1971: Surface thermal boundary condition for ocean circulation models, *Journal of Physical Oceanography*, **1**, 241-248
- Hasselmann, K., 1982: An ocean model for climate variability studies, *Progress in Oceanography*, **11**, 69-92
- Ikeda, M., 1990: Decadal oscillations of the air-ice-ocean system in the northern hemisphere, *Atmosphere-Ocean*, **28**, 106-139
- Krishnamurti, T.N., S-H Chu and W. Iglesias, 1986: On the sea level pressure of the southern oscillation, *Archives for Meteorology, Geophysics and Bioclimatology, Series A*, **34**, 385-425
- Lazier, J.R.N., 1980: Oceanographic conditions at O.W.S. Bravo

- 1964-1974, *Atmosphere-Ocean*, **18**, 227-238
- Levitus, S., 1982: Climatological atlas of the world ocean, NOAA Professional Paper 13, U.S. Department of Commerce: National Oceanic and Atmospheric Administration
- Manabe, S. and K. Bryan, 1985: CO<sub>2</sub>-induced change in a coupled ocean-atmosphere model and its paleoclimatic implications, *Journal of Geophysical Research*, **90**, 11689-11707
- Marotzke, J., 1990: Instabilities and multiple equilibria of the thermohaline circulation, Ph.D. thesis, Ber. Inst. Meeresk., Kiel, 194, 126 pp.
- Myers, P.G., 1991: Seasonal forcing and low-frequency variability of the thermohaline circulation, M.Sc. Thesis, McGill university
- Mysak, L.A. and D.K. Manak, 1989: Arctic sea-ice extent and anomalies, 1953-1984, *Atmosphere-Ocean*, **27**, 376-405
- Mysak, L.A., D.K. Manak and R.F. Marsden, 1990: Sea-ice anomalies observed in the Greenland and Labrador Seas during 1901-1984 and their relation to an interdecadal Arctic climate cycle, *Climate Dynamics*, **5**, 111-133
- Schlosser, P., G. Banisch, M. Rhien and R. Bayer, 1991: Reduction of deepwater formation in the Greenland Sea during the 1980's: Evidence for tracer data, *Science*, **251**, 1054-1056
- Schmitt, R.W., P.S. Bogden and C.E. Dorman, 1989: Evaporation minus precipitation and density fluxes for the North Atlantic, *Journal of Physical Oceanography*, **19**, 1208-1221
- Washington, W. and G. Meehl, 1989: Climate sensitivity due to increased CO<sub>2</sub>: experiments with a coupled atmosphere and ocean general circulation model, *Climate Dynamics*, **4**, 1-38
- Weaver, A.J. and E.S. Sarachik, 1990: On the importance of vertical resolution in certain ocean general circulation models, *Journal of Physical Oceanography*, **20**, 600-609
- Weaver, A.J. and E.S. Sarachik, 1991a: The role of mixed boundary conditions in numerical models of the ocean's climate, *Journal of Physical Oceanography*, **25**, 1470-1495
- Weaver, A.J. and E.S. Sarachik, 1991b: Evidence for decadal variability in an ocean general circulation model: An advective mechanism, *Atmosphere-Ocean*, **29**, 197-231
- Weaver, A.J., E.S. Sarachik and J. Marotzke, 1991a: Freshwater flux forcing of decadal and interdecadal variability, *Nature*, **353**, 836-838
- Weaver, A.J., J. Marotzke, P.F. Cummins and E.S. Sarachik, 1991b: Stability and Variability of the thermohaline circulation, *Journal of Physical Oceanography*, submitted
- Wetherald, R.T. and S. Manabe, 1972: Response of the joint ocean-atmosphere model to the seasonal variation of solar radiation, *Monthly Weather Review*, **100**, 42-59

Wright, D.G. and T.F. Stocker, 1991: A zonally averaged ocean model for the thermohaline circulation. Part I: Model development and flow development, *Journal of Physical Oceanography*, in press

### Figure Captions

**Figure 1.** a) — Restoring temperature ( $^{\circ}\text{C}$ ) at the southern boundary over the course of a year.

b) — Restoring temperatures for the basin over the course of a year: A — spring; B — summer; C — fall; D — winter.

**Figure 2.** a) — Meridional overturning streamfunction during the summer, at the end of the spin-up (Contour interval 2.0 Sv).

b) — As in a) except for winter.

c) — Zonal temperature profile during the summer, at the end of the spin-up (Contour interval 1.0  $^{\circ}\text{C}$ ).

d) — As in c) except for winter.

**Figure 3.** Density flux field ( $10^{-6}$   $\text{kg}/\text{m}^2\text{s}$ ) at the end of the spin-up during: a) — spring; b) — summer; c) — fall; d) — winter; and e) — an annual average. (Contour interval 1.0  $10^{-6}$   $\text{kg}/\text{m}^2\text{s}$ , except in d with 3.0  $10^{-6}$   $\text{kg}/\text{m}^2\text{s}$ )

f) — The absolute value of the ratio of the thermal and haline fluxes (Contour Interval 5.0).

**Figure 4.** Temporally averaged annual mean surface freshwater fluxes (metres/year) as diagnosed from the spin-up.

**Figure 5.** Surface freshwater fluxes (metres/year) as diagnosed from the spin-up for different times of the year: a) — spring; b) — summer; c) — fall; d) — winter.

**Figure 6.** Net surface heat flux ( $\text{W}/\text{m}^2$ ) averaged over the entire basin for Exp. 2 (*Fully Seasonal*): a) — 500 years of asynchronous integration; b) — 500 years of synchronous integration.

**Figure 7.** Net surface heat flux ( $\text{W}/\text{m}^2$ ) averaged over the entire basin during Exp. 3 (*Seasonal Temperature*) for a) — every summer for 6000 years of integration; b) — every winter for 6000 years of integration. c) — Power spectral density (using a 512 point fft) of the net

surface heat flux portrayed in Fig. 7a (Exp. 3) over the entire 6000 year integration. The x-axis corresponds to the number of cycles over this period;

d) — As in c) but for Fig. 7b (Exp. 3)

**Figure 8.** Meridional overturning streamfunction through an decadal oscillation of Exp. 3 (*Seasonal Temperature*):

a) — weakening phase of the oscillation;

b) — during existence of reverse cell;

c) — maximum strength phase of the oscillation;

d) — intermediate phase of the oscillation.

**Figure 9.** a) — The absolute value of the ratio of the thermal to the haline effects on the density flux from Exp. 3 (*Seasonal Temperature*). Annually averaged and averaged over an oscillation (Contour Interval 5.0)

b) — Density flux field ( $10^{-6}$  kg/m<sup>2</sup>s) into the basin. Annually averaged and averaged over an oscillation (Contour interval  $1.0 \cdot 10^{-6}$  kg/m<sup>2</sup>s).

**Figure 10.** a) — Net surface heat flux (W/m<sup>2</sup>) averaged over the basin for every winter of the 6000 years of integration of Exp. 4. (*Synchronous Seasonal Temperature*) b) — Difference field of zonal temperatures from Exp.'s 3 (*Seasonal Temperature*) and 4 during the summer. c) — As in b) but during the winter.

**Figure 11.** a) — As in Fig. 7a but for Exp. 5 (*Seasonal Freshwater Flux*). b) — As in Fig. 7c but for Fig. 11a (Exp. 5).

**Figure 12.** Kinetic energy density ( $10^{-1}$  kg/ms<sup>2</sup>) for

a) — Exp. 6 (*Perpetual Spring*); b) — Exp. 5 (*Seasonal Freshwater Flux*).

**Figure 13.** a) — As in Fig. 7a but for Exp. 7 (*Amplified Seasonal Temperature*). b) — As in Fig. 7c but for Fig. 13a (Exp. 7).

**Figure 14.** a) — As in Fig. 7a but for Exp. 8 (*Reduced Seasonal Temperature*). b) — As in Fig. 7c but for Fig. 14a (Exp. 8).

c) — Kinetic energy density ( $10^{-1}$  kg/ms<sup>2</sup>) for Exp. 8.

**Figure 15.** Poleward heat transport in petawatts ( $10^{15}$  W)

a) — Exp. 2 (summer(A) and winter(B)); b) — Exp. 1 (summer

and winter); c) — Exp. 3 (summer); d) — Exp. 3 (winter);

e) — Exp. 5 (summer and winter). Note that e) only examines the variability in the poleward heat transport over the decadal oscillation and not during a flush.

**Table 1** Vertical spacing used in all experiments. All depths are in meters.

Model Level	Depth of middle of vertical gridbox	Depth of bottom of vertical gridbox	$\Delta z$
1	25	50	50
2	87.5	125	75
3	175	225	100
4	287.5	350	125
5	425	500	150
6	600	700	200
7	825	950	250
8	1100	1250	300
9	1450	1650	400
10	1875	2100	450
11	2325	2550	450
12	2775	3000	450
13	3250	3500	500
14	3750	4000	500
15	4250	4500	500

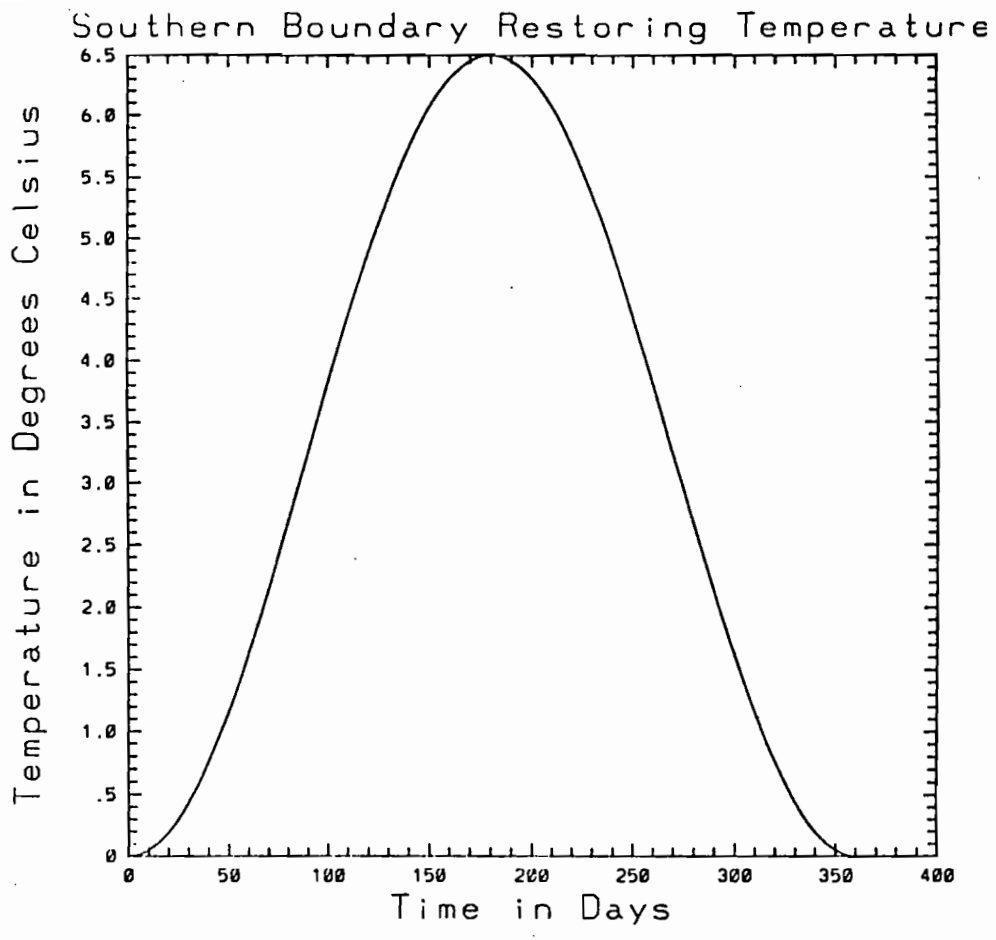
**Table 2** Characteristics of the 8 experiments: Column 1 - Experiment number; Column 2 - Restoring boundary condition used on temperature (seasonal or not); Column 3 - Flux boundary condition used on the salinity (seasonal or not); Column 4 - Tracer timestep used in the integration (days); Column 5 - States whether synchronous (S) or asynchronous (A) integration was used; Column 6 - The initial condition at the start of each experiment (ES implies end of spin-up); Column 7 - Maximum summer restoring temperature at the polar boundary (°C).

Exp.	Seasonal Cycle On Temp.	Freshwater Flux	Tracer Timestep (days)	S or A	Initial Condition	Summer Temp.
1	NO	NO	1.25	A	ES	0.0
2	YES	YES	2.5	A	rest	6.5
3	YES	NO	1.25	A	ES	6.5
4	YES	NO	0.25	S	ES	6.5
5	NO	YES	1.25	A	ES	0.0
6	NO	NO	1.25	A	ES	3.25
7	YES	NO	1.25	A	ES	9.0
8	YES	NO	1.25	A	ES	4.0

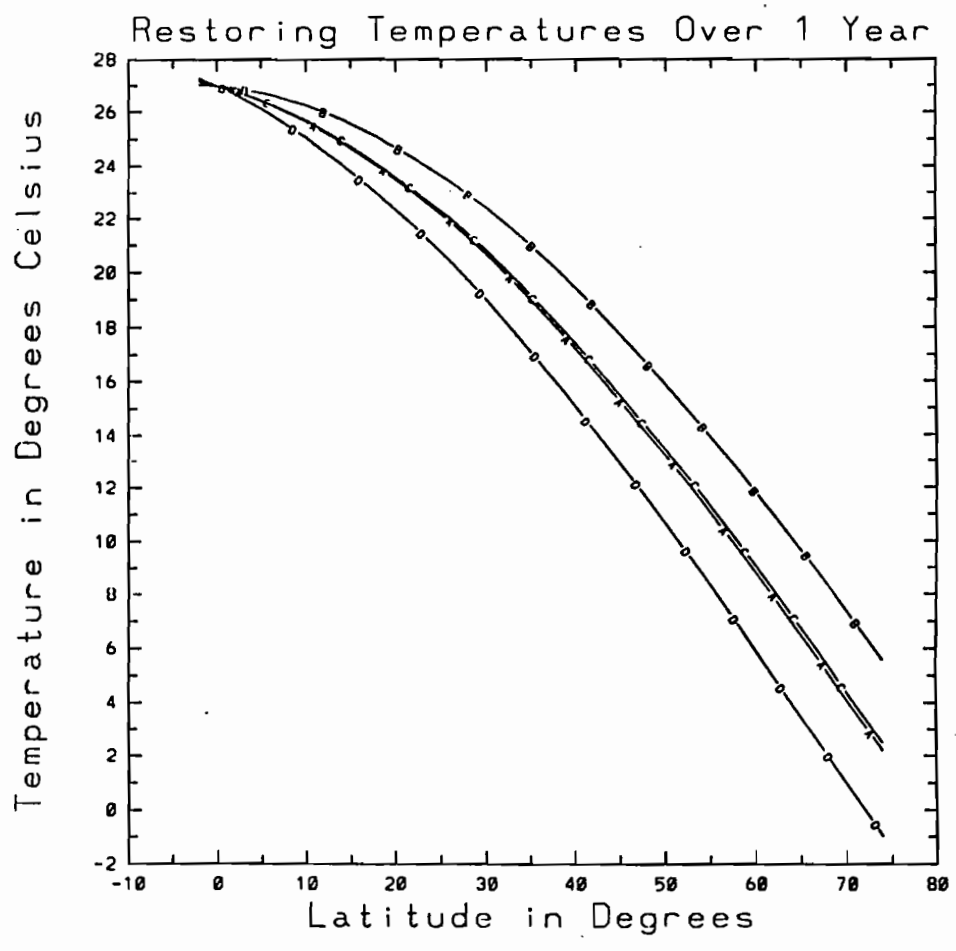
**Table 3** Characteristic timescales of variability (in years) of the 8 experiments. Also basin averaged bottom water temperatures at the end of those experiments that reached a seasonal equilibrium. The bottom water temperature for the spin-up has also been included. All temperatures in °C.

Experiment	Timescale	Bottom Water Temperature
spin-up	none	5.1
1	29.4	2.6
2	20.8	5.1
3	11.4	8.1
4	11.4	8.1
5	330.0, 13.0	no equilibrium
6	1700.0	no equilibrium
7	300.0, 11.4	no equilibrium
8	500.0, 8.3	no equilibrium

1a

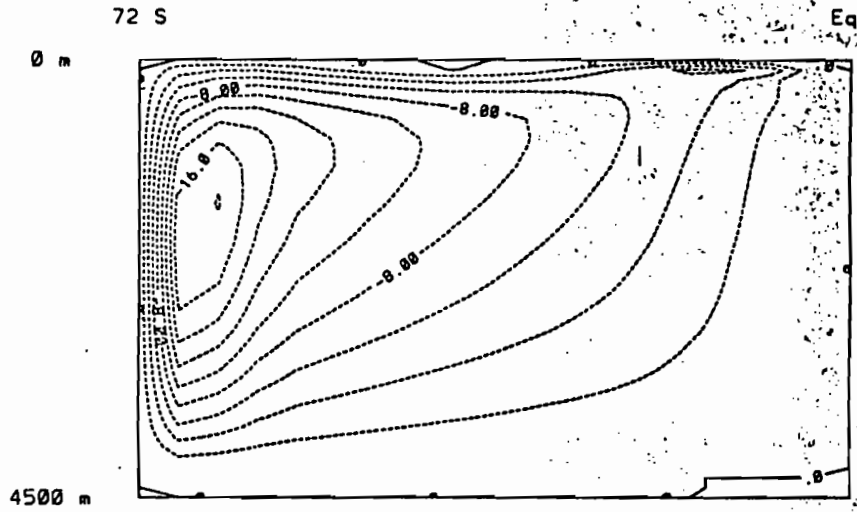


b



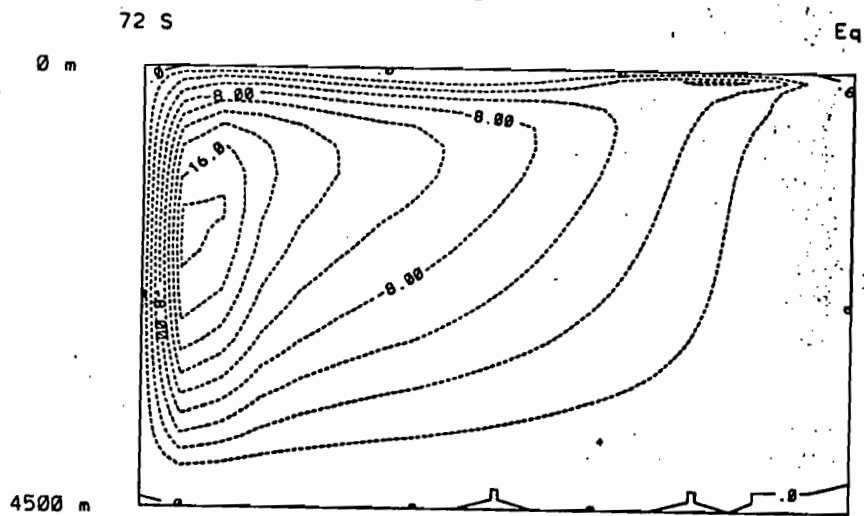
Overturning for Summer

2 a



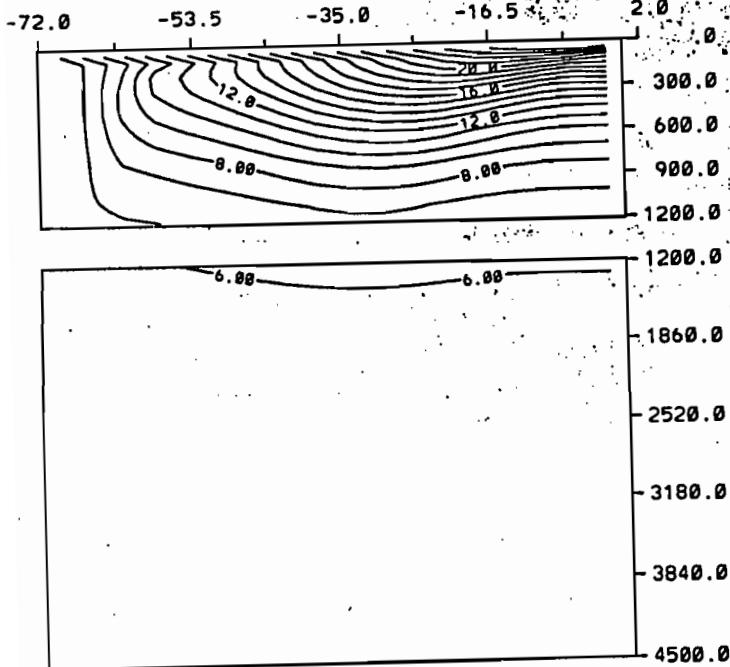
Overturning for Winter

b



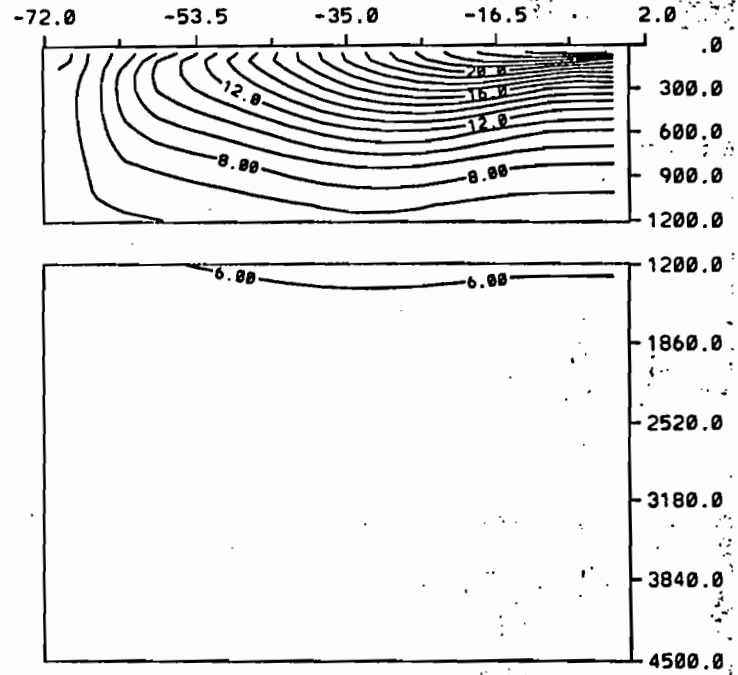
c

ZONAL TEMPERATURE FIELD FOR SUMMER

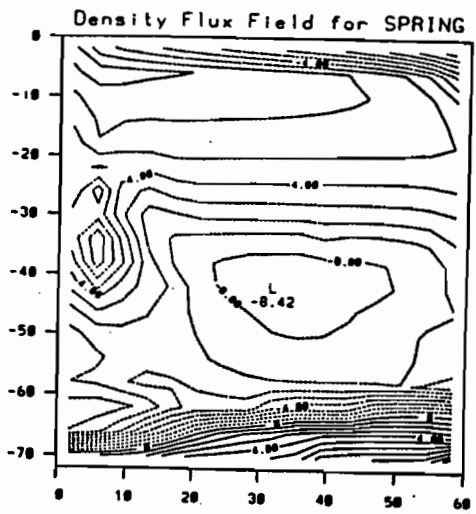


d

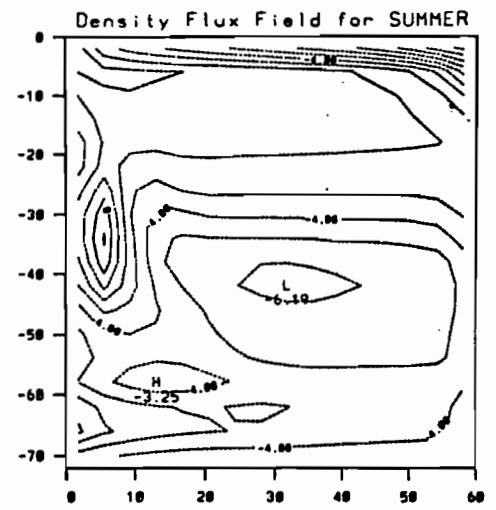
ZONAL TEMPERATURE FIELD FOR WINTER



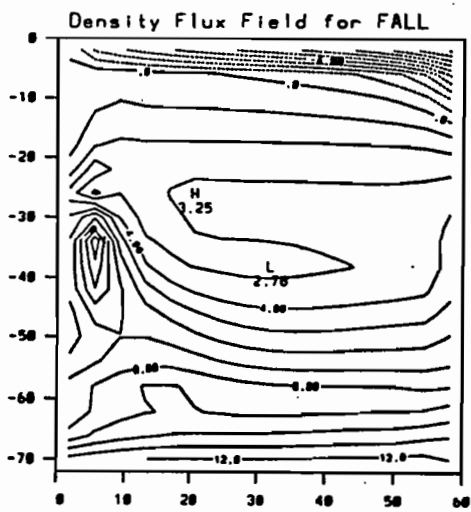
3a



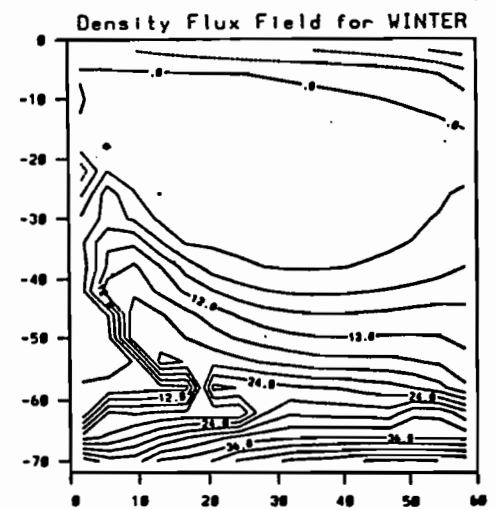
D



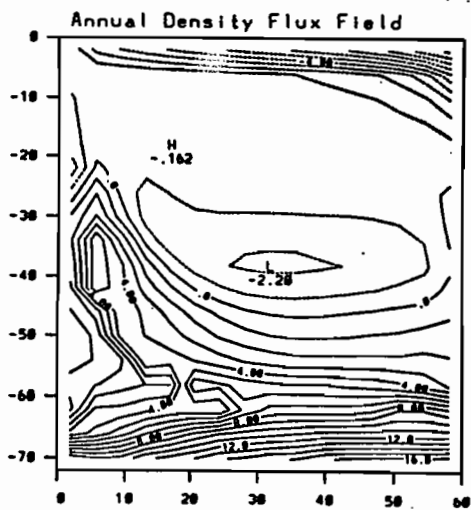
C



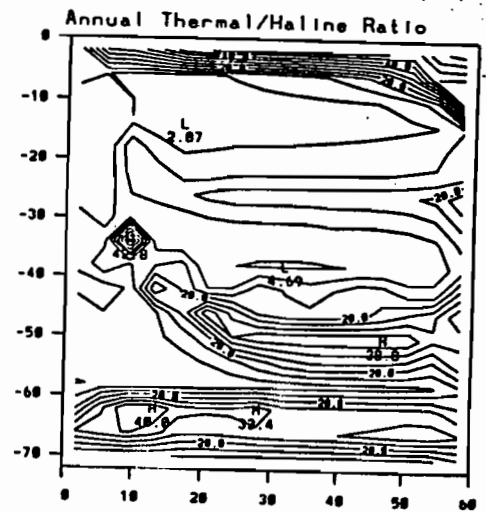
d



e

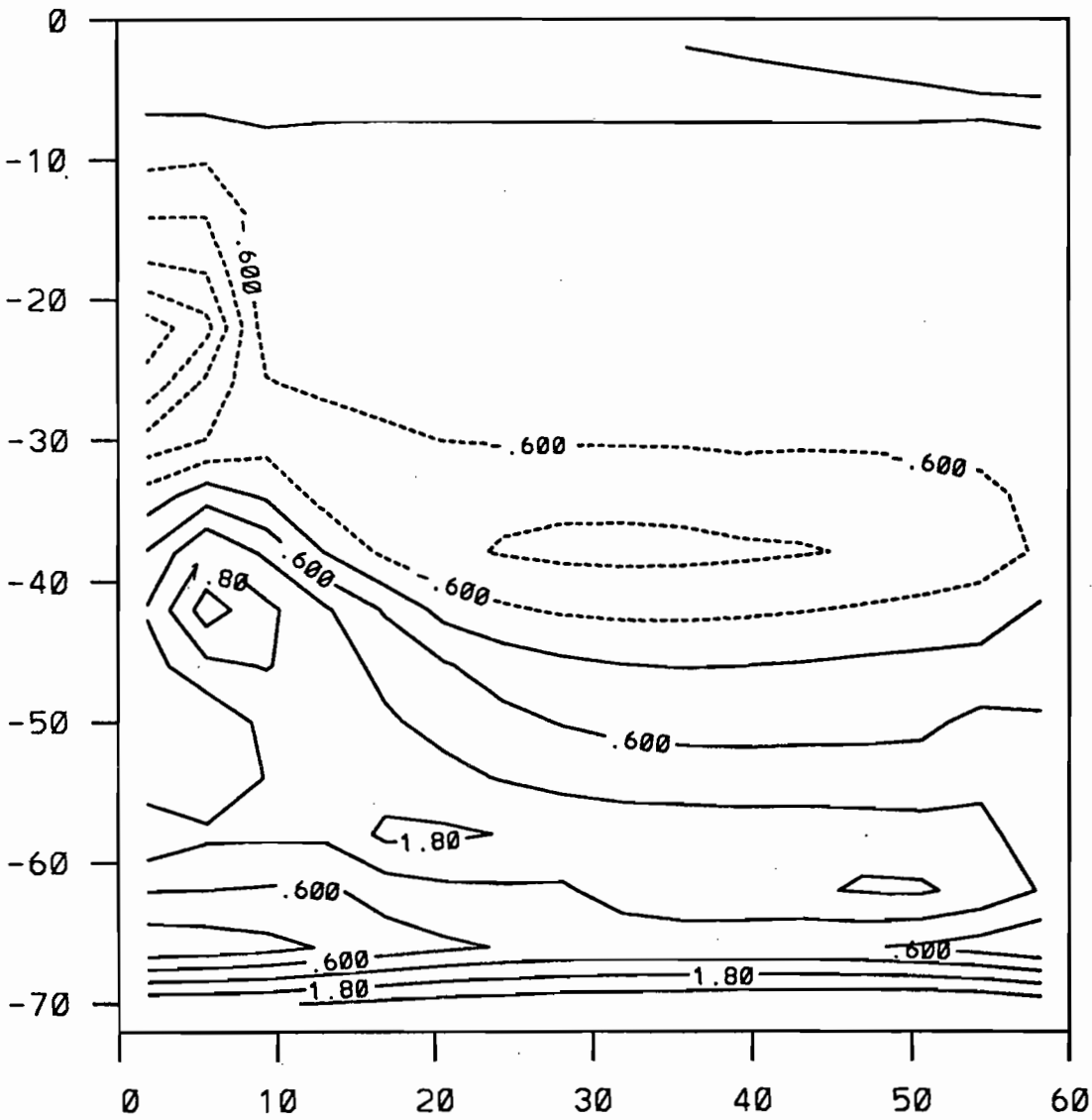


f

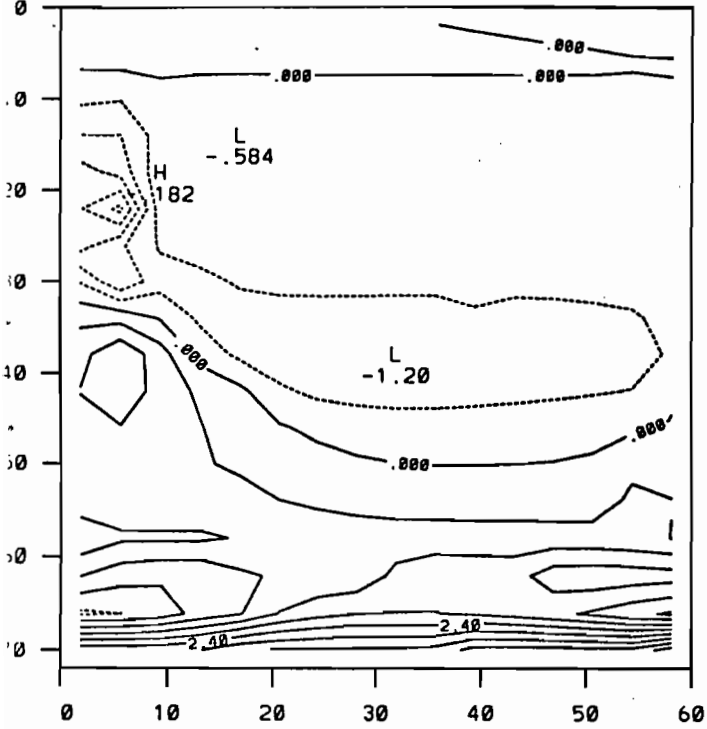


4

### ANNUAL FRESHWATER FLUX FIELD

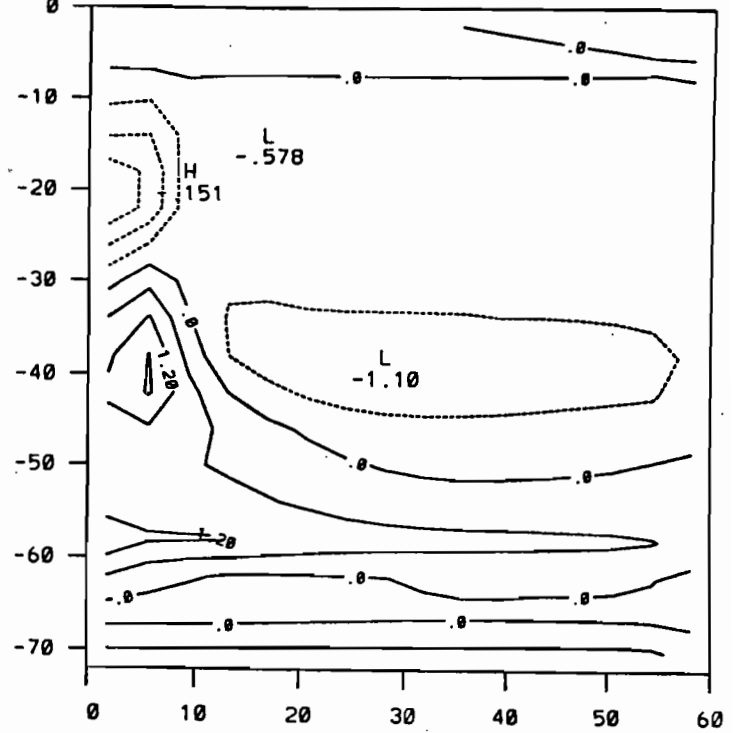


FRESHWATER FLUX FOR DAY 90



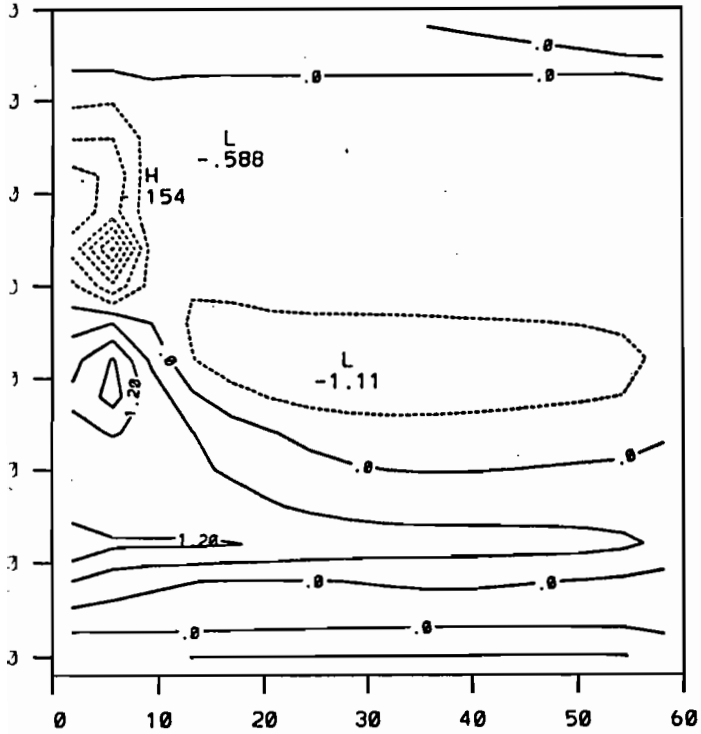
D

FRESHWATER FLUX FOR DAY 180



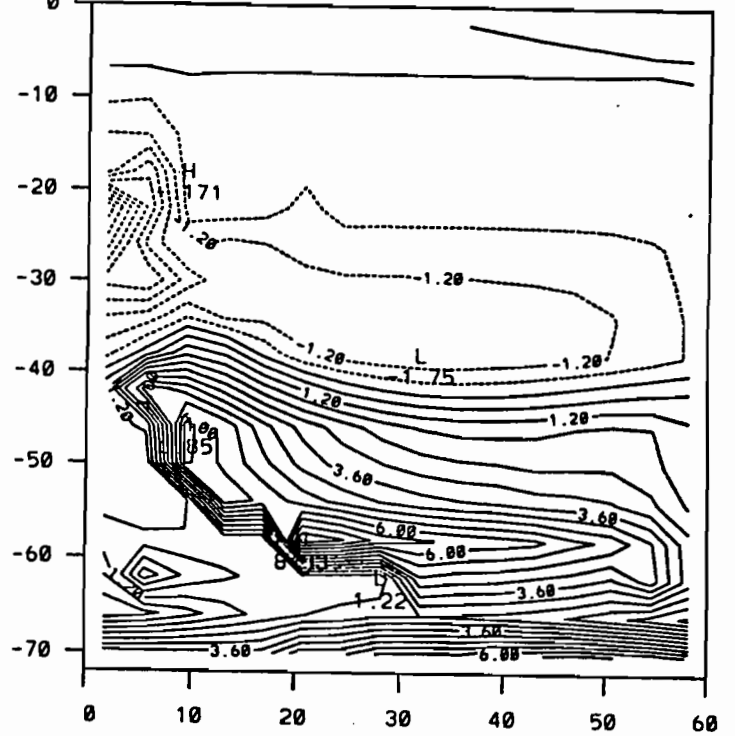
C

FRESHWATER FLUX FOR DAY 270

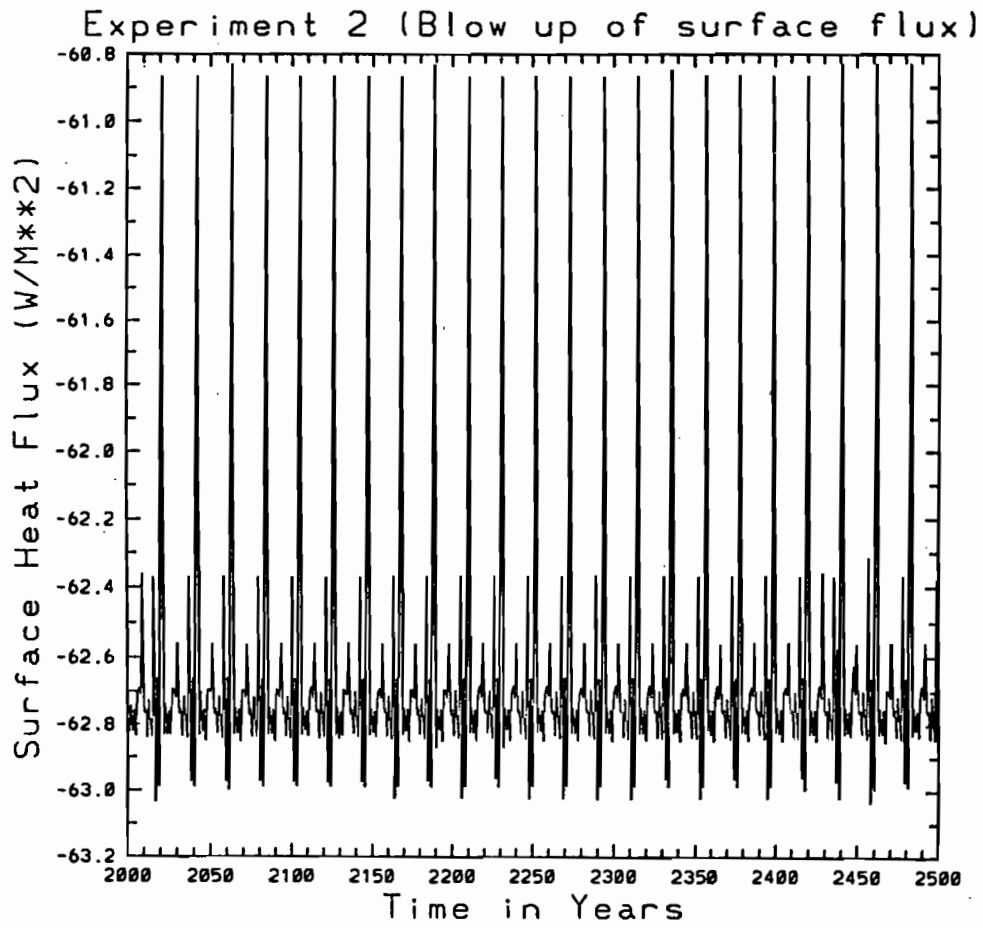


D

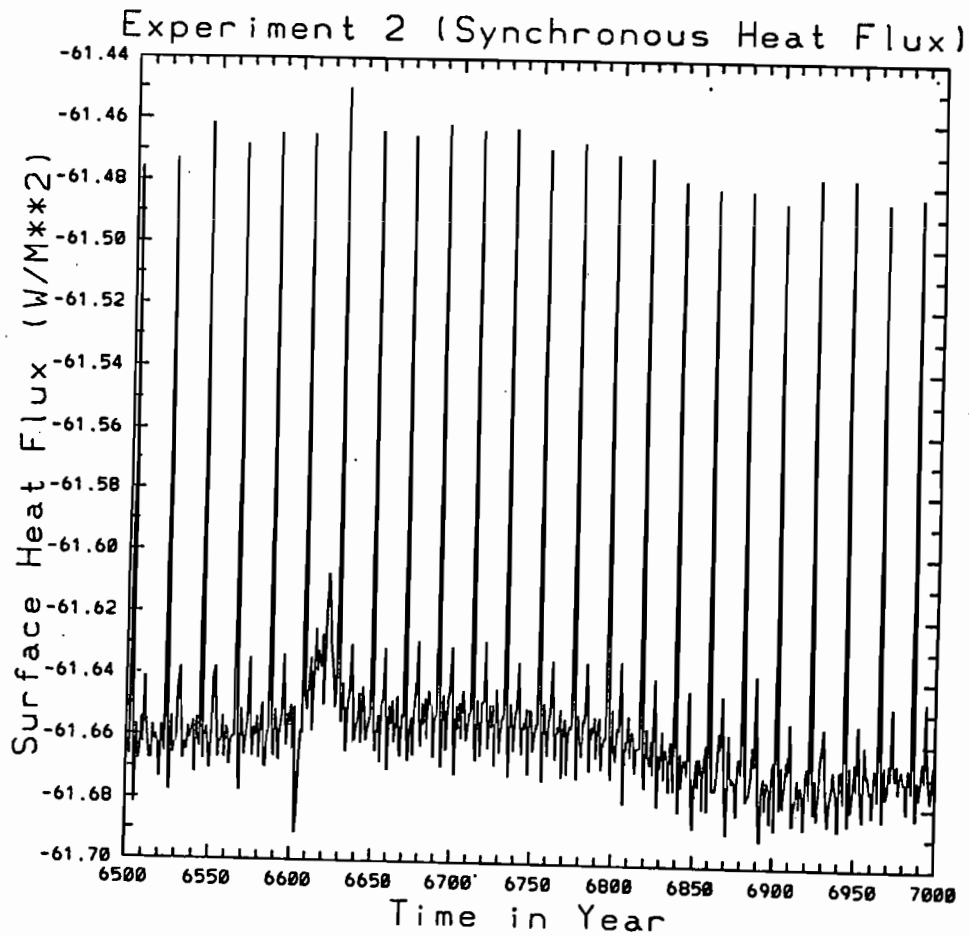
FRESHWATER FLUX FOR DAY 360



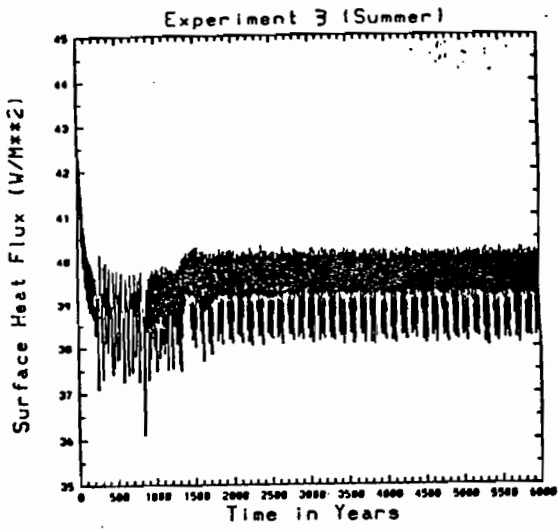
6a



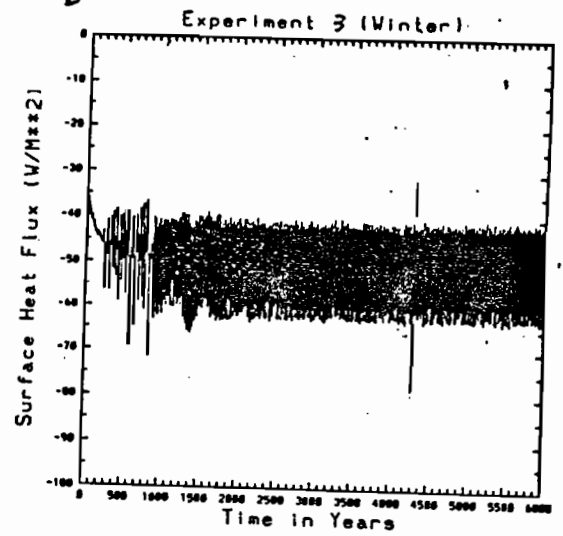
b



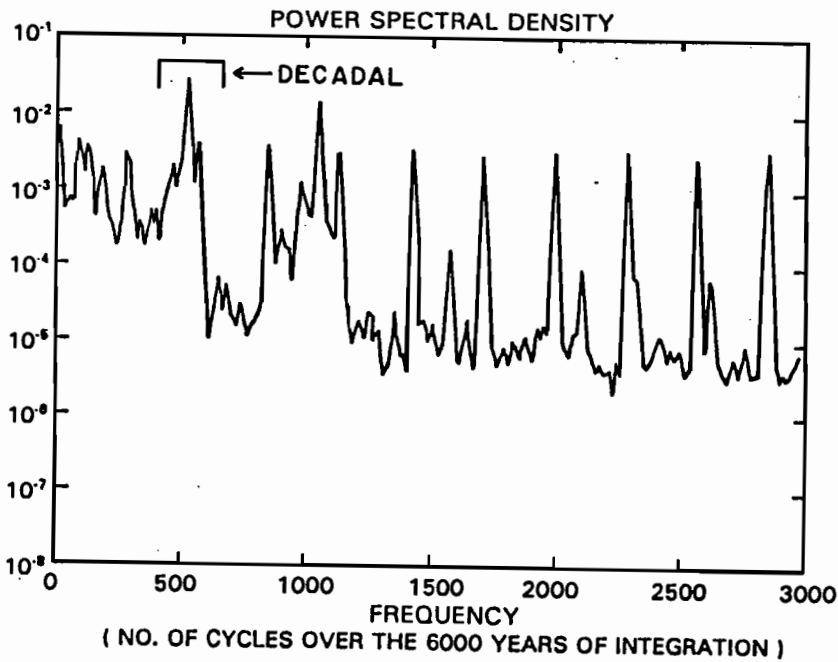
1a



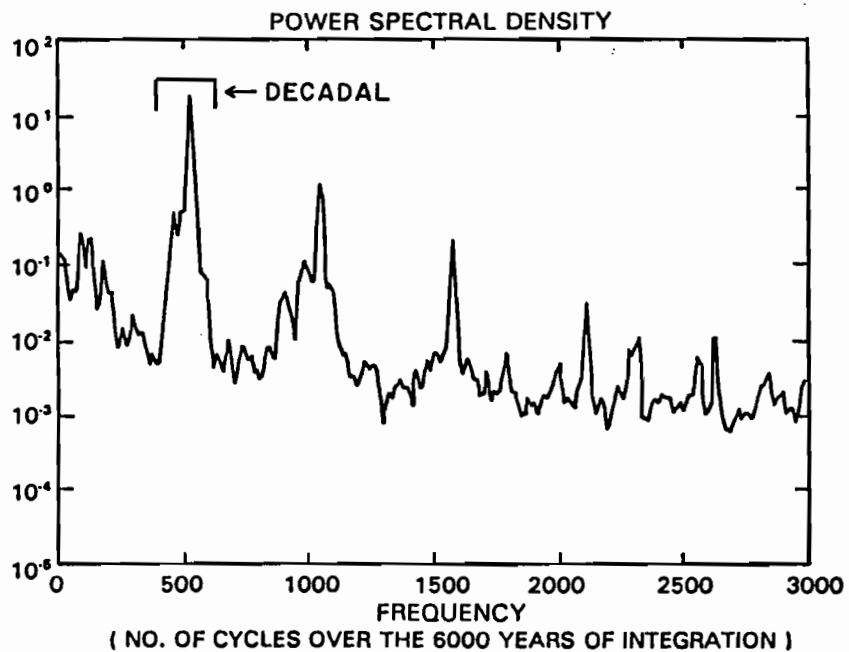
D



C

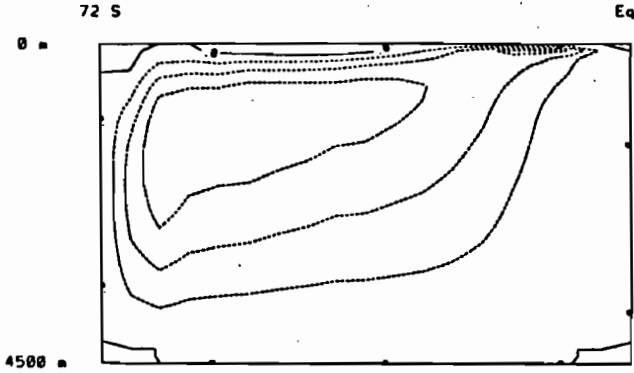


d



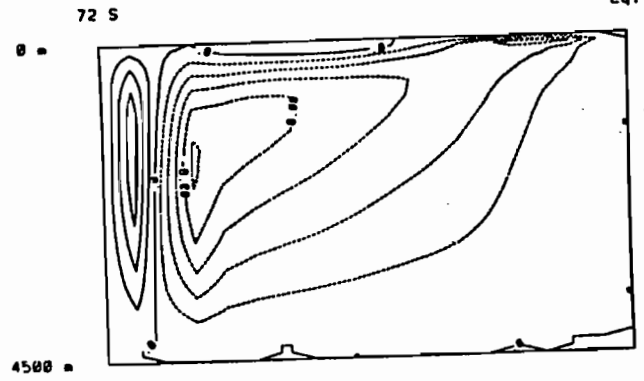
8a

Meridional Overturning at Year: 6003.00



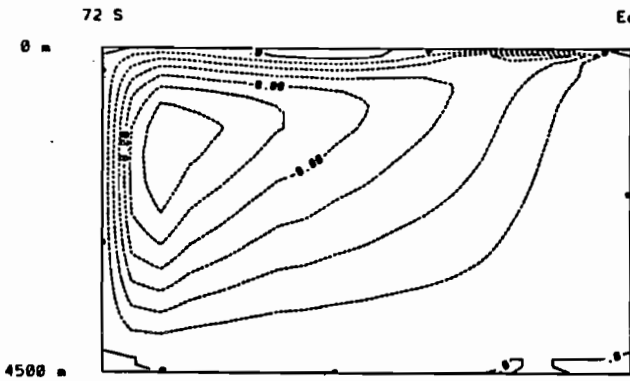
b

Meridional Overturning at Year: 6006.00



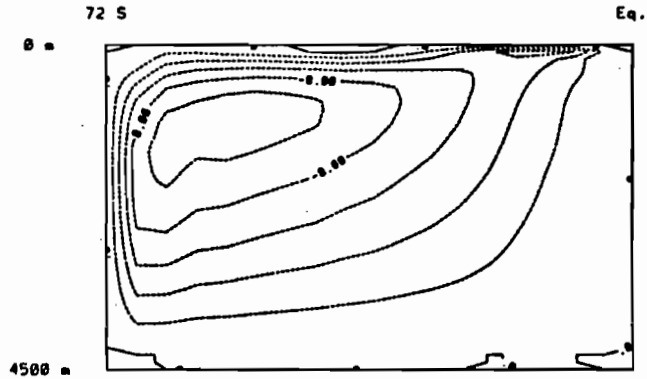
c

Meridional Overturning at Year: 6009.00



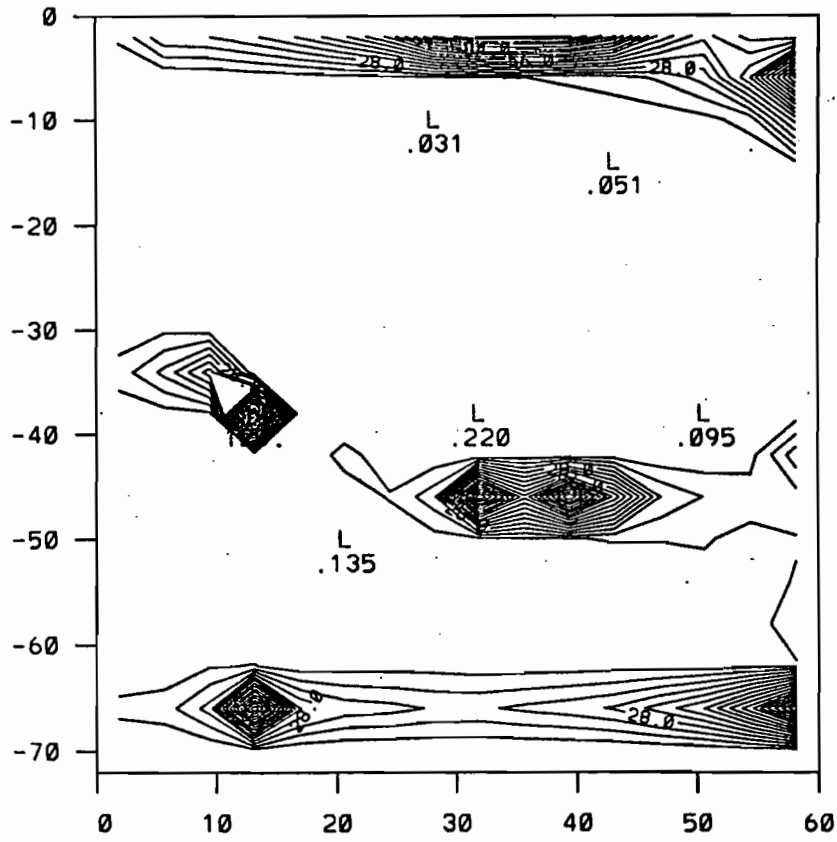
d

Meridional Overturning at Year: 6012.00



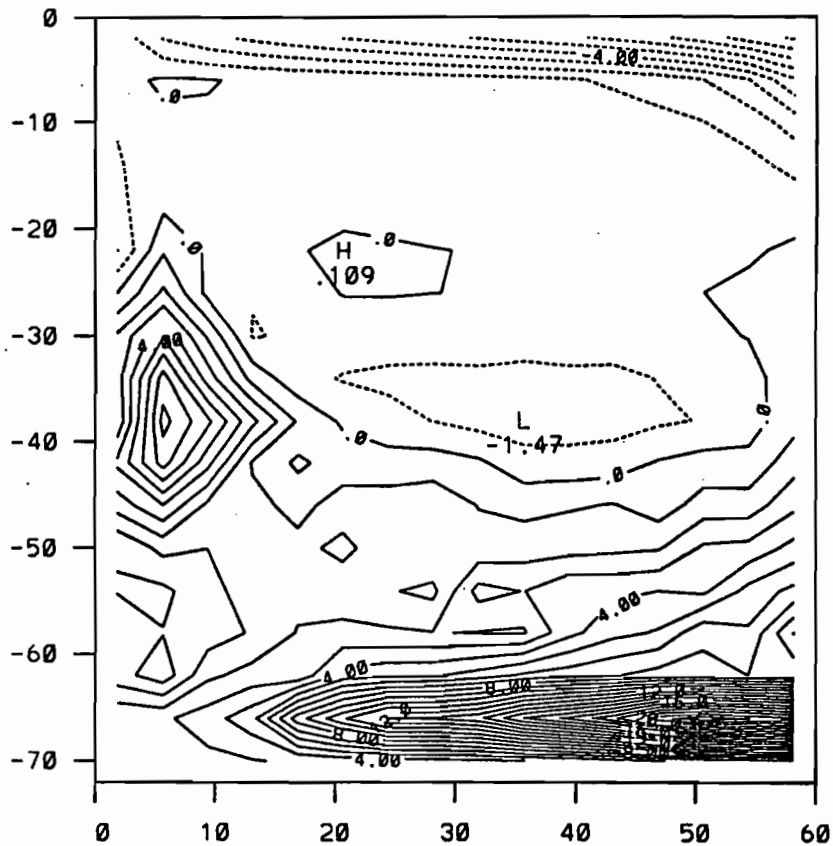
# Thermal/Haline Ratio

9a



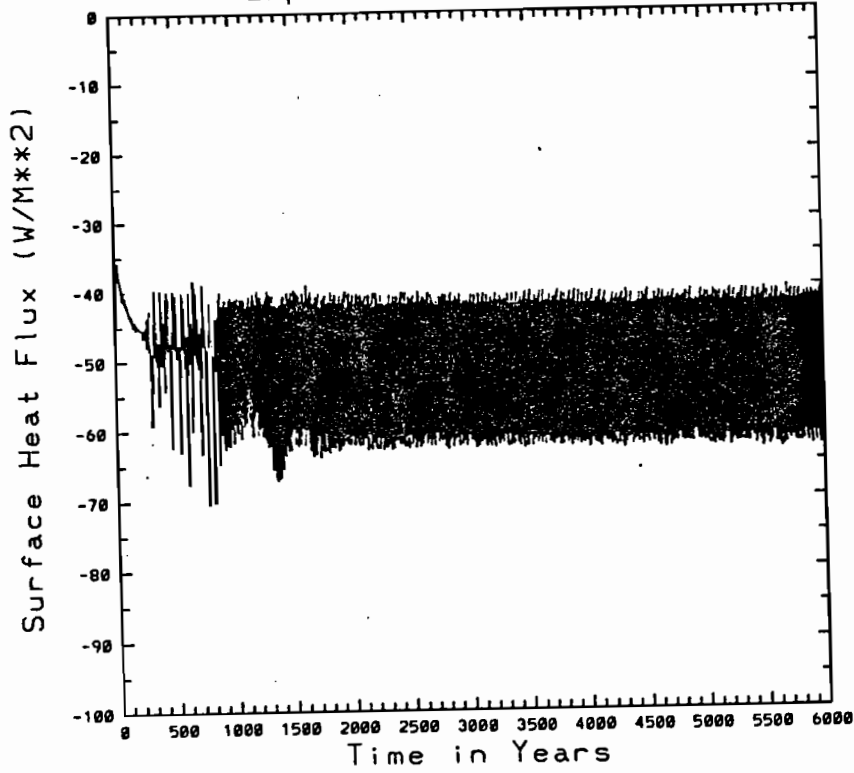
# Averaged Density Flux Field

b

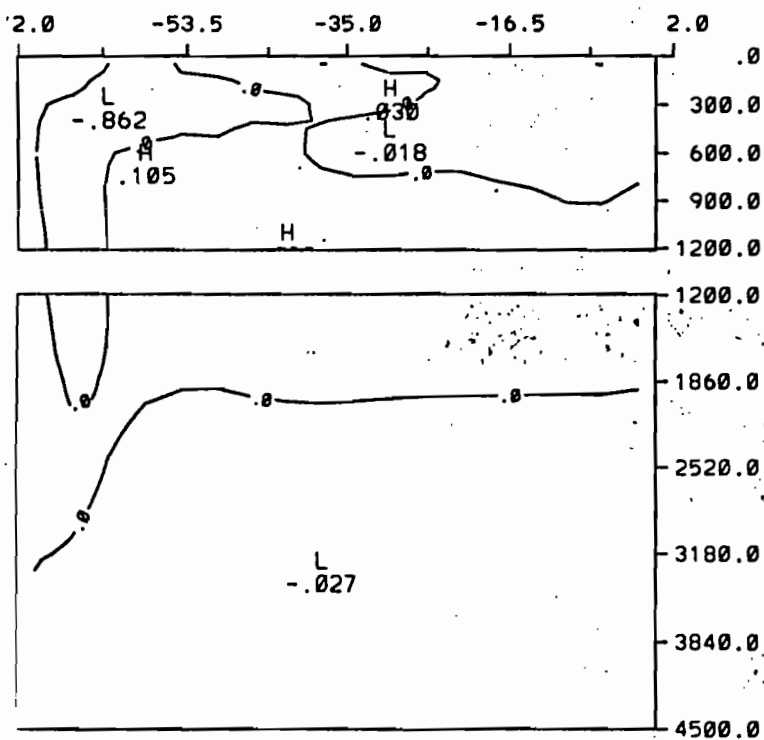


10a

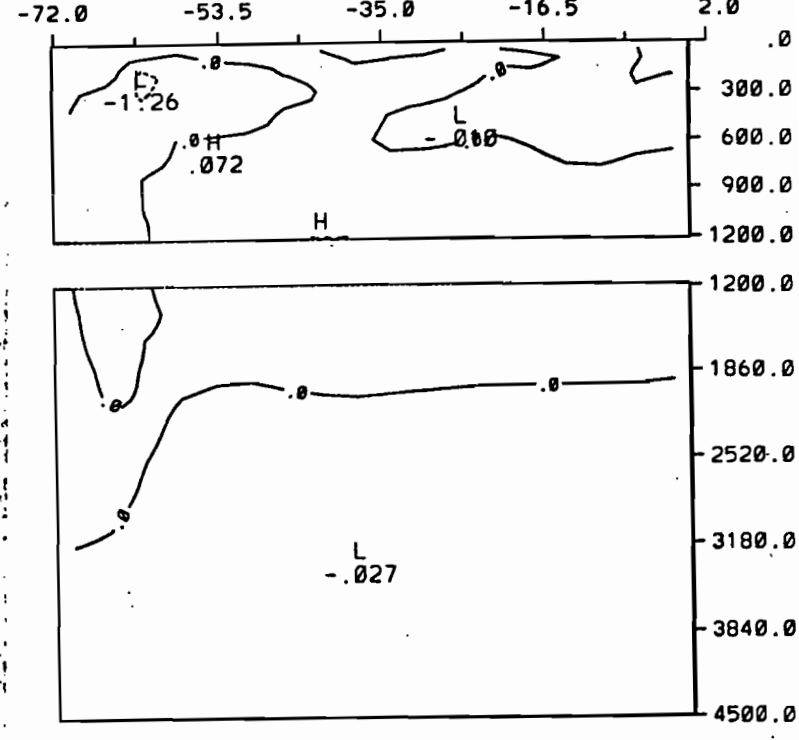
Experiment 4 (winter)



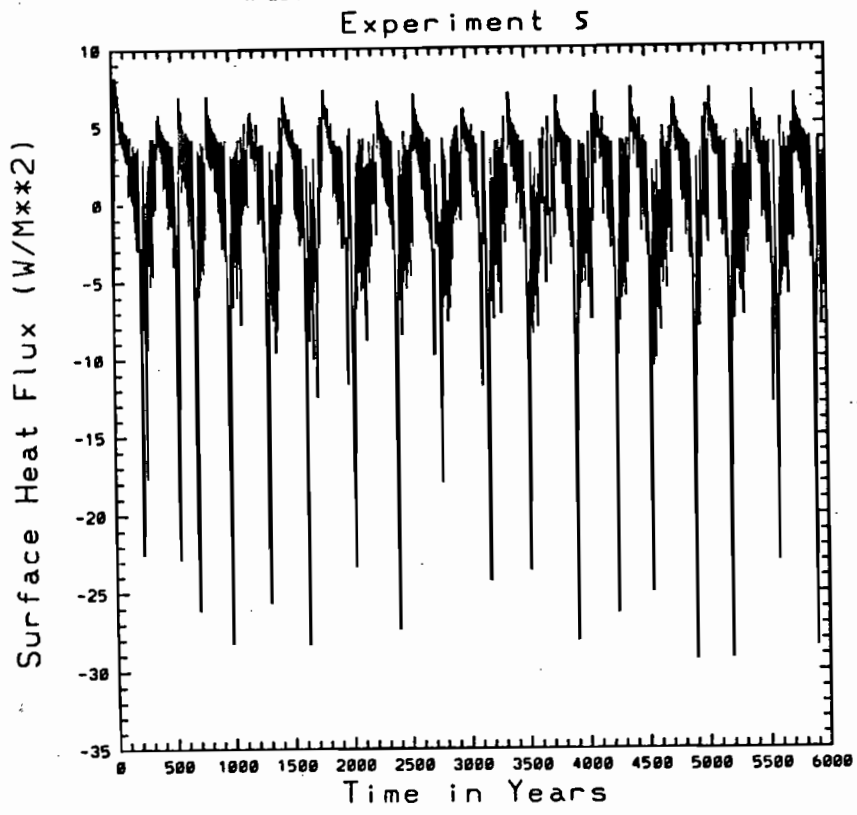
b ZONAL DIFFERENCE FIELD FOR SUMMER



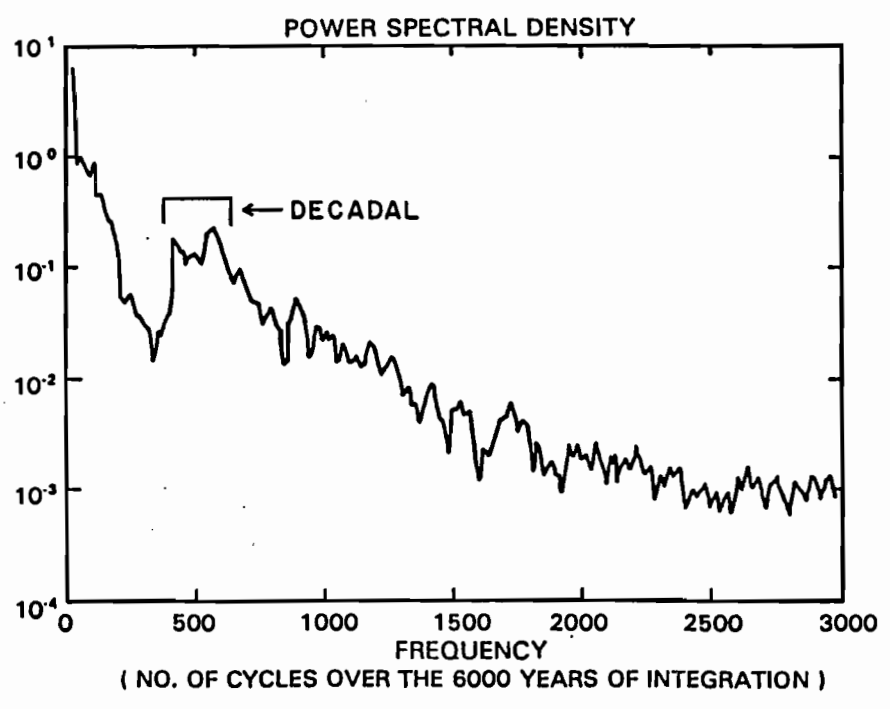
c ZONAL DIFFERENCE FIELD FOR WINTER



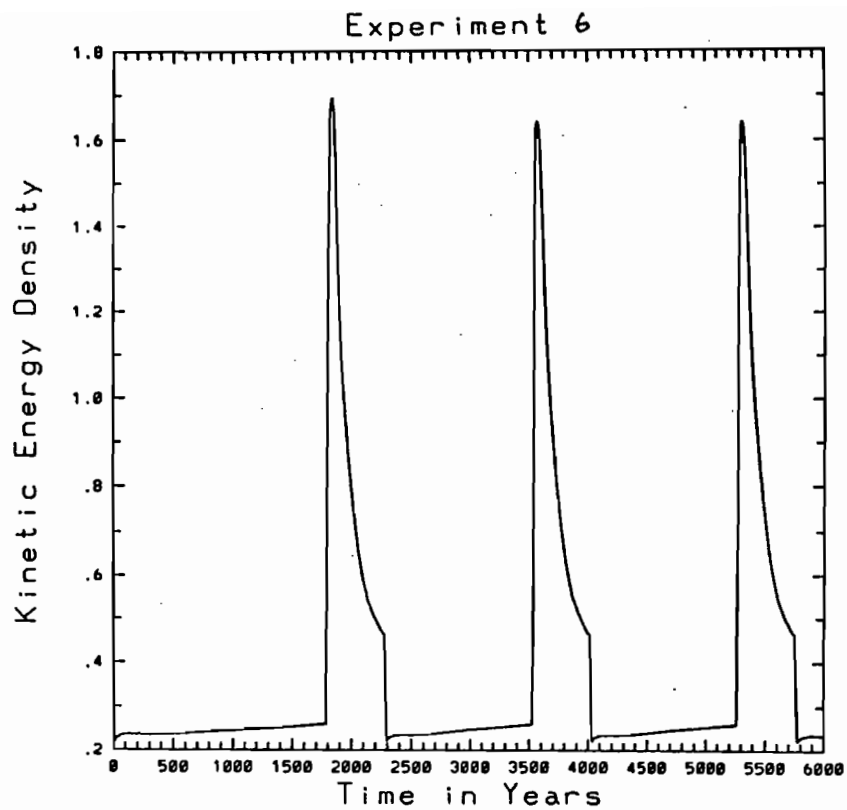
11 a



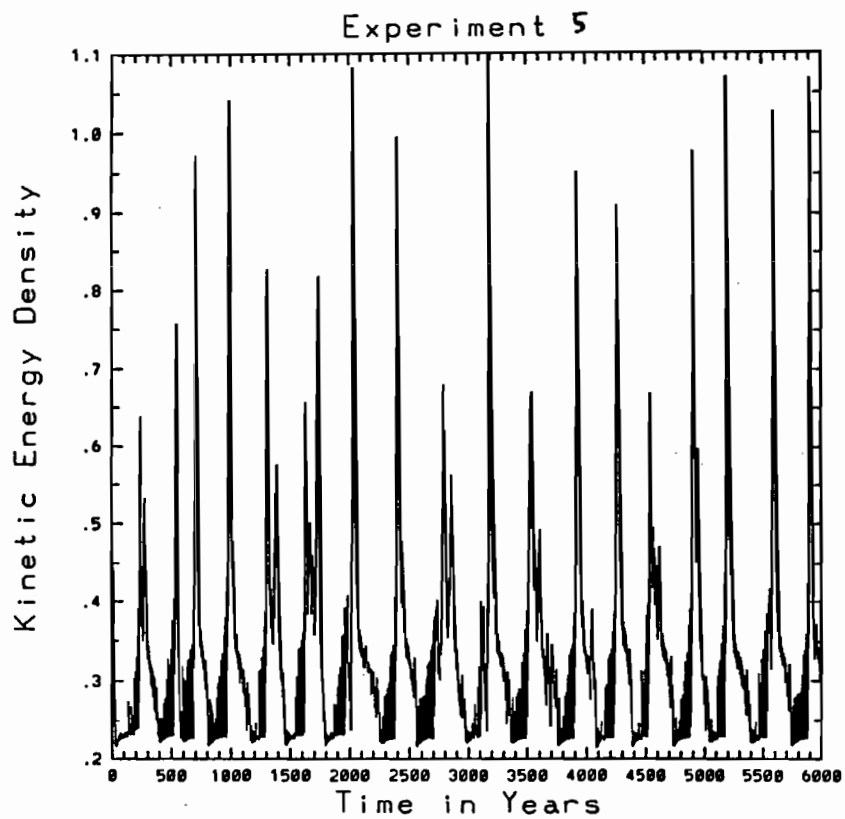
b



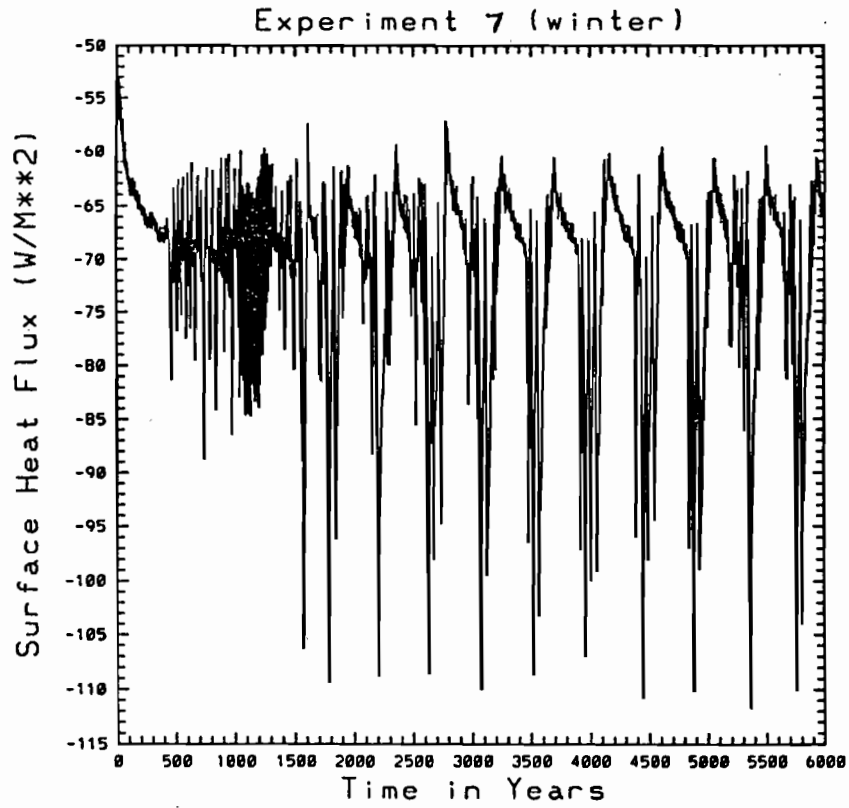
12 a



b



13 a



b

